UNIVERSITY OF OSLO
Department of geosciences
MetOs section

Impact of increased stratospheric water vapor concentrations on atmospheric radiative transfer

Master thesis in Geosciences Meteorology and oceanograpy

Jørgen Skredsvig Nilsen

10th June 2005

Abstract

Estimates are given of radiative forcings from various anthropogenic sources of stratospheric water vapor. These sources are direct emissions of water vapor from airplanes and the production of stratospheric H_2O by oxidation of anthropogenic methane. Preliminary comparisons with radiative forcings derived by other researchers are done by perturbing an everywhere fixed value of stratospheric water vapor of 6 ppmv by 0.7 ppmv. Fair agreement with published results is found, both for SW and LW radiative forcings. The uniform perturbation setup is further used as a basis for sensitivity studies of stratospheric coolings attributable to single model-layer increases in stratospheric water vapor levels. As for the study of aircraft emissions, future scenarios involving both traditional subsonic as well as high-altitude supersonic air traffic are used, and radiative forcings are calculated for the years 2025 and 2050 versus present day. Changes in stratospheric H_2O from methane oxidation are estimated via two different pathways. The first involves the use of direct observational data from the HALOE instrument covering the years 1991-1999. Based on available time series of human methane emissions, stratospheric water vapor production through the oxidation of methane for several periods of time is calculated. The second method uses output of water vapor production by methane oxidation from the Oslo CTM-2 model. These methane datasets are interpolated into a T21L60 grid, and radiative forcings, as well as stratospheric temperature changes are modeled. The temperature responses are shown to depend crucially on the vertical profile of water vapor used, with lower-stratospheric warmings as a potential result of applying the methane-induced water vapor changes. The radiative forcing from these two anthropogenic sources combined is found make up around 10% of the radiative forcing from the total increase in stratospheric water vapour since 1960, thus confirming the forcing from increased stratospheric water vapour to be partly of human origin.

Contents

Chapter 1

Introduction

Since the late 19th century, the global mean temperature has risen by an estimated 0.6°C. Paleoclimatic analyses indicate that this represents the greatest warming in any century during the past 1000 years, with the 1990s as the warmest decade of the millennium. Thus, climate change is indeed a reality, and there is general agreement within the scientific community that global warming is at least partly a consequence of human activities. Possible human-induced climate changes are primarily tied to the abrupt, and largely ongoing increases in emissions of greenhouse gases, most notably CO_2, following the industrial revolution some 200 years ago. The subject of climate change and its ongoing and future consequences arises intensive interest and debate within a variety of academic circles, as well as in politics and economy, thereby penetrating into almost every thinkable aspect of human society.

This particular thesis deals with the subject of *atmospheric radiative transfer*, i.e the study of interaction between radiation and the earth-atmosphere system. By the aid of numerical models simulating processes such as absorption and emission taking place in the atmosphere, one is able to produce reliable estimates of e.g. the warming potential arising from increased concentrations of greenhouse gases. Over the past decades, a large number of papers have dealt with estimating the external forcings on the climate system arising from anthropogenic emissions of greenhouse gases. The warming potential of the principal greenhouse gases such as CO_2,CH_4, N_2O and CFCs has been a topic of large interest, and is therefore considered to be fairly accurate. However, not all species potentially able to impact the climate are equally well mapped, neither in terms of quantification, origin or distribution. One such species with a possible impact on the overall global warming is water vapor residing in the stratosphere, whose ability to add to the greenhouse effect has only recently received interest among researchers within atmospheric sciences.

Over the past decades, a positive trend in the concentration of stratospheric water vapor (SWV) has been observed. On the basis of both long-term aircraft and balloon measurements as well as more recent time series from the HALOE and SAGE-II satellites, Rosenlof et al. (2001) estimated the vertically averaged increase to 2 ppmv since the 1950s, equal to 1% per year. Taking into account the present value of SWV of 4-6 ppmv, this clearly represents a significant perturbation. However, all the governing mechanisms

of this increase are not understood. Oxidation of methane in the stratosphere is known to be one important source of SWV. On the other hand, the well documented increase in tropospheric methane concentrations of 0.55 ppmv over the past 45 years is capable of explaining an increase in SWV of 1.1 ppmv at most. Aircraft emissions of water vapor in the lower stratosphere have obviously also risen sharply during this period, but only a small percentage of the overall observed increase is attributable to intensified air traffic. Although these two anthropogenic sources cannot account for all of the observed SWV increase, any climatic impact of the corresponding SWV change can be considered as a direct anthropogenic forcing. Various suggestions have been made in attempting to explain the remaining part of the observed trend, that is, the SWV increase that is not directly attributable to neither methane oxidation nor aircraft emissions. Rosenlof et al. (2001) point toward the hypothesis of a large-scale change in stratospheric circulation and stratosphere-troposphere exchange that may increase the stratospheric residence time of i.e CH_4, thus increasing methane oxidation and ultimately SWV generation. Also, the observed increase in tropospheric temperatures clearly favors higher levels of water vapor in the troposphere, and may in principle act as a source of SWV through a tropospheric-stratospheric exchange that may or may not have strengthened. Although these mechanisms are far from understood, there is current consensus that the SWV increase may be viewed partly as a climate forcing through aircraft emissions and increased CH_4, and partly as a feedback from increased tropospheric temperatures and possible corresponding changes in troposphere-stratosphere circulation. On the background of the observed perturbations of SWV levels, a number of papers have in recent years focused on estimating the radiative forcing that arises from increased SWV levels.(e.g Forster and Shine (1999),Smith et al. (2001)) Also, one seeks to fully understand the role of SWV increase versus ozone depletion in order to better explain the observed cooling of the lower stratosphere in the past decades. As for studying the impact of SWV on radiative forcing, the main motivation is clearly to establish an estimate of its potential to add to the radiative forcing already present due to increased levels of well known greenhouse gases such as CO_2, CH_4 and CFCs. It has been suggested in Forster and Shine (2002) that the forcing from the SWV trend of the past 40 years is roughly 75% of that of the CO_2 increase from preindustrial to present day concentrations. The changes in SWV since 1980 are simliarily thought to account for a radiative forcing of 40% of CO_2 (Forster and Shine (1999)). In this thesis, we will focus mainly on providing estimates of the radiative forcing attributable to various scenarios of increased stratospheric water vapor levels. We will begin by applying an idealized water vapor perturbation, i.e a change in SWV levels from 6ppmv to 6.7ppmv. This particular experimental setup has been used to calculate radiative forcings in a number of papers, most notably by Forster and Shine (1999), thus making it an obvious choice in terms of model inter-comparison and validation. Finally, we will try to come up with estimates of the direct anthropogenic component of the forcing from increased SWV by calculating radiative forcings from projected future air traffic and from production of SWV by oxidation of methane since preindustrial times.

Chapter 2

Theory and concepts

The various gases in the earth's atmosphere can roughly be grouped by the variations in space and time of their concentrations. Some species, like CO_2 exhibit fairly constant mixing ratios in the vertical and are generally deemed as well-mixed, whereas others, such as H_2O and O_3 show distinct variation with height. In addition come cloud particles and aerosols, which vary greatly, both in space and time. The atmospheric concentrations of several of the radiatively active gases such as CO_2 and CH_4 have risen significantly since the dawn of the industrial era, due to combustion of fossil fuels and greater biogenic emissions from a growing human population, respectively. In addition, human activity has also provided the atmosphere with gases that do not exist in nature, the most important ones being the chlorofluorocarbons (CFCs). These play a significant role, both by adding to the earth's greenhouse effect and by contributing to the observed decay of stratospheric ozone, especially at high latitudes. Thus, to come up with reliable model estimates of the climate change potential from a changing atmospheric environment, one must pursue both a thorough quantification of the changes taking place as well as an understanding of the subsequent interactions between the various atmospheric constituents. Last, but not least, a solid knowledge in the field of atmospheric radiative transfer is vital in order to provide realistic model representations as a basis for reliable estimates of the warming potential of changes in atmospheric constituents.

2.1 Composition and thermal structure of the atmosphere

To properly describe the interaction of solar radiation and the atmosphere, one needs to understand the composition and thermal structure of the atmosphere. Based on current standard nomenclature, the atmosphere is vertically stratified into four distinct regions. These are the troposphere, the stratosphere, the mesosphere and the thermosphere. It is in the troposphere that we find nearly all the water vapor, as well as clouds and precipitation. As for water vapor, however, a marked decline in concentration as a function of height is observed throughout the troposphere, resulting in very dry conditions at the tropopause. The main thermal property of the troposphere is a marked decrease in temperature from about 288K at the surface to around

220K at the with a lapse rate of around 6.5 K km^{-1}. This lapse rate is nearly constant in the lower and middle levels of the troposphere, but begins to decrease in the upper troposphere. The *tropopause*, i.e the transition level between the troposphere and the stratosphere is normally defined as the height where the lapse rate drops below 2K km^{-1}. As for the stratosphere, which extends vertically from 12-15km up to 50 km, the temperature remains fairly constant from above the tropopause and up to around 30 km. Above this level, the temperature then rises gradually up to around 270 K at the stratopause, mainly due the local heating effect of the ozone layer, which is confined to heights of around 20-25 km. In terms of water vapor, the stratosphere is known to be very dry, with concentrations in the area of 4-6 ppmv with little vertical variation.

2.2 Radiative transfer - fundamental concepts

Generally speaking, the earth-atmosphere system receives its energy from the sun as visible or ultraviolet radiation, and re-emits energy as thermal IR radiation and sensible and latent heat. For the system as a whole, there must clearly exist a balance between incoming and outgoing radiation for the climate to remain stable. The study of radiative transfer and climate change ultimately deals with the mechanisms maintaining this balance, and indeed with the diagnose and quantification of factors that may or may not contribute to perturbing it. A key term in this sense is the greenhouse effect, which occurs naturally in the climate system by the absorption of thermal radiation emitted from the surface ("heat trapping") by gases such as H_2O, CO_2,CH_4 etc. In order to come up with reliable estimates of both ongoing and future warming by increased human emissions of many of these gases, a solid theoretical framework is crucial. This section will present some of the fundamental equations describing the transfer of radiation in the atmosphere, as well as their applications in numerical simulations. Solar radiation, commonly referred to as shortwave radiation, has its energy peak concentrated around wavelengths of 0.5μm. Thermal infrared radiation, denoted as long-wave radiation, has its maximum energy concentrated at longer wavelengths at around 10μm. Since there is little overlap between the two, they are normally treated separately, thus greatly simplifying the analysis of atmospheric radiative transfer.

2.2.1 Atmospheric scattering and absorption of solar radiation

On the average, the top of the atmosphere receives 342 W/m^2 of solar energy, out of which 31 % is immediately reflected back into space. The remaining 235 W/m^2 is partly absorbed by the atmosphere and partly by the surface of the earth (land and ocean). The atmospheric transfer of solar radiation is greatly influenced by scattering (redirectioning) of sunlight both by single molecules and by larger particles such as dust, smoke, sulfur-aggregates etc. These are commonly referred to as aerosols, and are generally thought to contribute to a cooling of the earth's surface by dimming the incoming sunlight, thus reducing the energy available for absorption.

Generally, the transfer of solar intensity in a plane-parallel atmosphere may be written:

$$\frac{\Delta I(z;\mu,\phi)}{\Delta z/\mu} = -\beta_e I(z;\mu,\phi) + \beta_s F_\odot e^{-\tau/\mu} \cdot P(\mu,\phi;-\mu_0,\phi_0)/4\pi + \beta_s \int_0^{2\pi}\int_{-1}^{1} I(z,\mu',\phi') \cdot P(\mu,\phi;\mu',\phi')/4\pi d\mu' d\phi' + \beta_a B[T(z)] \quad (2.1)$$

where μ and ϕ are the zenith and azimuthal angles of the outgoing radiation, β_e,β_s and β_a denote the extinction, scattering and absorption coefficients (of unit $[length^-1]$, respectively. $F_\odot$ denotes the solar irradiance at the top of the atmosphere. $P(\mu,\phi;\mu',\phi')$ denotes the phase function, i.e the redirectioning by aerosols, cloud droplets and molecules of the incoming intensity from direction (μ',ϕ') to the outgoing direction (μ,ϕ). Finally, B is the Planck radiation from within the layer Δz

This equation forms the basis for computations dealing with the transfer of radiation in the atmosphere, and is of crucial importance both in numerical simulations as well as in remote sensing applications.

2.2.2 Atmospheric solar heating rates

Several of the atmospheric constituents, such as H_2O, O_3 and CO_2 absorb radiation in the visible and near infrared, thereby generating heat. Ozone plays a key role in warming the stratosphere through the absorption of UV radiation with subsequent emission of thermal IR radiation. Stratospheric water vapor also has an impact in this sense, but as we shall see in subsequent sections, its potential for producing heat by absorption of visible and UV radiation is more than outweighed by its absorption and emission properties in the thermal IR spectral area. In terms of solar heating rates, it is the tropospheric water vapor that by far contributes the most, mainly due to the high concentrations of water vapor in the lower troposphere.

Assume a plane-parallel atmosphere of differential thickness Δz illuminated by the sun. We denote the upward and downward solar fluxes by $F^\uparrow$ and $F^\downarrow$, respectively, and define the net flux at height z as:

$$F(z) = F^\downarrow(z) - F^\uparrow(z) \quad (2.2)$$

The absorption of solar flux clearly causes the flux to decrease when proceeding downward vertically. In other words, the (negative) flux change in a layer is proportional to the heating generated in the layer, i.e:

$$\frac{\partial T}{\partial t} = -\frac{1}{\rho C_p}\frac{\Delta F(z)}{\Delta z} \quad (2.3)$$

In numerical models, this computation is normally carried out by grouping the entire solar spectrum into a number of spectral intervals, and then performing the calculations of fluxes for each of the spectral intervals by means of some computational method. This is a fairly complicated task, involving both the absorption by key atmospheric species, as well as scattering by molecules and aerosols and reflection from the surface. The solar fluxes later referred to in this thesis are computed by means of an implementation of the *discrete ordinate method*.

2.2.3 The discrete ordinate method

The discrete ordinate method was first developed by Chandrasekhar (1950), and has later been refined into a powerful numerical tool in terms of computing fluxes in atmospheres containing complicating elements such as aerosols and clouds (Liou, 1973). The basic idea consists of discretizing the equation of radiative transfer, which is transformed, via a series of mathematical manipulations, into a computer-friendly matrix formulation of a set of differential equations. Our brief outline of the procedure starts with rewriting (2.1) using $\mathbf{\Omega} = (\mu, \phi)$ and the optical depth, τ rather than the previous three variables (z;μ,ϕ):

$$\mu \frac{dI(\tau, \mathbf{\Omega})}{d\tau} = I(\tau, \mathbf{\Omega}) - \frac{\tilde{\omega}}{4\pi} \int_{4\pi} I(\tau, \mathbf{\Omega}') P(\mathbf{\Omega}, \mathbf{\Omega}') d\Omega' - \frac{\tilde{\omega}}{4\pi} F_{\odot} P(\mathbf{\Omega}, -\mathbf{\Omega}_0) e^{-\tau/\mu_0} + (1 - \tilde{\omega}) B[T(\tau)] \tag{2.4}$$

Where the optical depth is given by

$$\tau = \int_z^{\infty} \beta_e dz' \tag{2.5}$$

and the term $\tilde{\omega}$ denotes the single scattering albedo. We next consider the azimuth-independent part of the diffuse intensity component, and replace the integral with a summation term. In this particular case, we may also omit the radiation term. This allows us to rewrite (2.4) as

$$\mu_i \frac{dI(\tau, \mu_i)}{d\tau} = I(\tau, \mu_i) - \frac{\tilde{\omega}}{2} \sum_{j=-n}^{n} I(\tau, \mu_j) P(\mu_i, \mu_j) a_j - \frac{\tilde{\omega}}{4\pi} F_{\odot} P(\mu_i, -\mu_0) e^{-\tau/\mu_0}, \quad i = -n, ..., n \tag{2.6}$$

where a_j define quadrature weights satisfying $\sum_j a_j = 2$
To simplify, we define

$$c_{i,j} = \frac{\tilde{\omega}}{2} a_j P(\mu_i, \mu_j), \quad j = -n, ..., 0, ..., n \tag{2.7}$$

and further

$$b_{i,j} = \begin{cases} c_{i,j}/\mu_i & i \neq j \\ (c_{i,j} - 1)/\mu_i & i = j. \end{cases}$$

This allows us to rewrite (2.6) in matrix notation as:

$$\frac{d}{d\tau} \begin{bmatrix} \mathbf{I}^+ \\ \mathbf{I}^- \end{bmatrix} = \begin{bmatrix} \mathbf{b}^+ & \mathbf{b}^- \\ -\mathbf{b}^- & -\mathbf{b}^+ \end{bmatrix} \begin{bmatrix} \mathbf{I}^+ \\ \mathbf{I}^- \end{bmatrix} \tag{2.8}$$

where

$$\mathbf{I}^{\pm} = \begin{bmatrix} I(\tau, \pm\mu_1) \\ I(\tau, \pm\mu_2) \\ \vdots \\ I(\tau, \pm\mu_n) \end{bmatrix} \tag{2.9}$$

and $\mathbf{b}^{\pm}$ refers to elements in connection with $b_{i,j}$ and $b_{i,-j}$ We have established a first order differential equation for $\mathbf{I}^{\pm}$ which can be solved numerically by means of well-known methods in linear algebra. To summarize, we have, via a series of mathematical manipulations, gone from the radiative transfer equation (2.1) and transformed it into the matrix formulation of the discrete ordinate method (2.11). The latter equation serves as a basis for model simulations of the transfer of solar radiation in the atmosphere.

2.2.4 SW model description

For the short-wave flux computations, a modified version of the discrete ordinate method (Stamnes et al. (1988)) is used. The calculations are performed using 8 streams. The model includes absorption by H_2O and O_3 as well as Rayleigh scattering and absorption and scattering by clouds. The spectral resolution varies over the solar spectrum, with high resolution below $2\mu m$ and lower resolution for wavelengths above $2\mu m$. The solar spectrum is divided into four main bands within which transmission functions for the principal absorbers are calculated by means of exponential-sum fitting.

For radiative transfer calculations, we use ECMWF data in T21 resolution ($5.625° \times 5.625°$) for temperatures, ground pressures, albedo, relative humidities and cloud cover. These are given as monthly averages for 3-hour intervals (00-03 GMT, 03-06 GMT,etc.) thus providing 8 sets of radiative fluxes per monthly run; one set for each of these given time intervals. For all purposes in this thesis, we create and apply monthly diurnal averages either as standalone fields or as as a basis for computing annual averages when needed.

The vertical layers are defined by the use of hybrid sigma-pressure levels, i.e using global pressure values to define the uppermost layers, and sigma-coefficients to determine all the below layers affected by terrain-induced surface pressure variations. For most of the simulations carried out, we use 60 vertical levels, ranging from the ground up to 0.11 hPa. This stratification provides high vertical resolution in the stratosphere, which is obviously convenient when working primarily with SWV. In terms of notation, the 3-D resolution obtained when working with a T21 horizontal grid using 60 vertical layers is conventionally referred to as T21L60-resolution.

2.3 Atmospheric long-wave radiative transfer

The earth-atmosphere-system reflects about 30% of the incoming solar radiation at the top of the atmosphere and absorbs the remaining part. For the radiative equilibrium to be maintained, this absorbed radiation is re-emitted as thermal infrared radiation. The emission spectrum of thermal IR radiation is shown to be close to that of a blackbody with a temperature of

around 255K, which is some 33 degrees below the actual global mean surface temperature. This surface warming is due to the natural greenhouse effect, i.e the heat trapping by absorption and re-emission of outgoing long-wave radiation by key greenhouse gases such as water vapor, CO_2, CH_4, etc. The study of thermal infrared radiation transfer in the atmosphere deals largely with quantifying the degree of absorption of this radiation by these atmospheric constituents, as well as estimating the warming potential associated with increased concentrations of greenhouse gases due to human activity.

The fundamental equations for upward and downward fluxes of atmospheric thermal infrared radiation are normally written in the form:

$$F_\nu^\uparrow(\tau) = \pi B_\nu(\tau_*) T_\nu^f(\tau_* - \tau) - \int_\tau^{\tau_*} \pi B_\nu(\tau') \frac{d}{d\tau'} T_\nu^f(\tau' - \tau) d\tau' \tag{2.10}$$

$$F_\nu^\downarrow(\tau) = \int_0^\tau \pi B_\nu(\tau') \frac{d}{d\tau'} T_\nu^f(\tau - \tau') d\tau' \tag{2.11}$$

The first term in the expression for the upward flux is the contribution from the surface emission weakened by absorption up to the level(τ) in question. This attenuation is represented by the diffuse transmittance T_ν^f. The second term represents the contributions from all below layers in terms of their Planck fluxes $B_\nu(\tau)$ and the corresponding local rate of change of transmittance. The latter may be thought of as a weighting function, with distant layers below being weighted lightly compared to closer layers. The expression for the downward flux is similar to this term, although the direction and limits of the integral are obviously different. These expressions may then be integrated over all wave numbers ν to model the full transfer of thermal infrared radiation in the atmosphere.

2.3.1 Atmospheric infrared cooling rates

Analogously to the solar heating rates discussed in section 2.2.2, we may also define the *infrared cooling rate* which arises due to the loss of heat to space by the atmosphere. Defining the net infrared flux at a given level z by

$$F(z) = F^\uparrow(z) - F^\downarrow(z) \tag{2.12}$$

gives the infrared cooling rate as:

$$\frac{\partial T}{\partial t} = -\frac{1}{\rho C_p} \frac{dF(z)}{dz} \tag{2.13}$$

In this sense, water vapor emission serves to cool the troposphere and the lower stratosphere, whereas ozone, as a consequence of the vertical placement of the ozone layer, warms the lower stratosphere and cools the upper stratosphere. The greatest cooling rates, however, are known to arise in the vicinity of cloud tops of middle and low clouds in the troposphere.

2.3.2 Broadband models

The fundamental idea behind broadband emissivity calculations is to use the Stefan-Boltzmann law instead of Planck fluxes for the computation of

infrared fluxes and heating rates. Using the path length u rather than optical depth as the vertical coordinate, we may define the *isothermal broadband flux emissivity* as:

$$\epsilon^f(u,T) = \int_0^\infty \pi B_v(T)[1 - T_\nu^f(u)]\frac{d\nu}{\sigma T^4} \tag{2.14}$$

This can be thought of as the degree of attenuation (between 0 and 1) of the total infrared flux emitted from a body of temperature T observed at a distance u from the emitting object. Flux calculations in broadband models are essentially based upon calculating the broadband flux emissivity for each of the principal atmospheric absorbers, most notably H_2O,CO_2 and O_3. Such numerical calculations are carried out by discretizing (2.9) into a desired number of bands, N:

$$\epsilon^f(u_j,T) = \sum_i \pi B_{\tilde{\nu},i}(T)[1 - T_{\tilde{\nu},i}^f(u_j)]\frac{\Delta\nu_i}{\sigma T^4} \;\; j = 1,2,...,N \tag{2.15}$$

Where the index i corresponds to the enumeration of the species considered. If one considers water vapor emissivity, for instance, one may set u_1=u_{H_2O} and then use already computed spectral transmittances for the water vapor bands in question. The beforehand computation of transmittances is typically done by line-by-line codes or band models. In spectral regions with significant band overlap, such as the H_2O rotational band overlap with the 15μm CO_2-band, a slight modification of the above expression is required. The standard procedure in such cases is to regard the transmittance in overlap regions as a product of the individual transmittances, i.e:

$$T_\nu(\bar{u}_{H_2O}, \bar{u}_{CO_2}) = T_\nu(\bar{u}_{H_2O})T_\nu(\bar{u}_{CO_2}) \tag{2.16}$$

This relation, valid for monochromatic radiation only, may then be used to express the emissivity in overlap regions in terms of individual emissivities and a correction term.

2.3.3 The OBIR model

The earlier version of OBIR was constructed by Stordal(1988) and is a broad band model for use in the infrared region. The model uses an emissivity formulation based on the work of Ramanathan[1976] for calculating radiative fluxes in the entire infrared spectral region. It includes the effects of all the gases of radiative importance in the infrared :H_2O, CO_2, N_2O, O_3 and CH_4 and CFCs. The main improvements provided in the 1995 version of OBIR consist of a refined vertical integration scheme for absorptivity and emissivity terms as well as the inclusion of the 14μm absorption band of ozone.

As for the water vapor representations, the spectral interval from 0-2200 cm^{-1} is divided into three main bands and six sub-bands. Also, the water vapor absorption continuum in the 500-1200 cm^{-1} is included. For CO_2, the 15μm band is included, and , and for O_3, the main band at 9.6μm as well as the weaker 14 um band are included. Altogether, about 50 bands are represented in the model for all species considered.

As is the case for most broad band models, the largest limitation of the OBIR is the treatment of band overlap. Most of the CFCs overlap with water vapor only, and in this case, one multiplies the absorptivity of one of the overlapping bands with the transmission of the other overlapping band. In this case, transmissions from the sub-bands of water vapor are used, except for overlap with CO_2, where a combination of water vapor sub-band transmissions is used. The overlap between N_2O and water vapor and between CH_4 and water vapor applies transmission for water vapor described by *Rodgers and Walshaw*[1966]. For overlap between gases other than water vapor, transmission calculations are carried out on the basis of exponential reduction of band strengths as a function of distance from the band centers in question.

Clouds are included in the OBIR model, and their effect is parametrized by means of combining the clear sky radiative flux and the flux from a cloud with variable emissivity. There are three cloud layers in the model, these are denoted as high, middle and low clouds. Random overlap between clouds in the tree layers is assumed, and the parametrization of the layers also allows variable emissivities. The input data used are once again the ECMWF data in T21L60 resolution.

2.4 Radiative forcing

The concept of radiative forcing can be briefly summarized as the change in the balance between incoming and outgoing radiation in the earth-atmosphere system. A positive radiative forcing generally tends to warm the surface of the earth while a negative forcing tends to cool it. Such a prescribed change in surface temperature is normally estimated using *general circulation models* (GCM). However, the estimates of surface temperature changes from different GCMs tend to vary greatly, primarily due to differences in the representation of climate feedback mechanisms of the various GCMs. Thus, looking exclusively at surface temperature changes predicted by GCMs may obscure our understanding of the fundamental warming or cooling potential of different atmospheric species. To simplify the quantification of different radiative components' ability to warm or cool the earth, the following definition of the radiative forcing concept has been established by IPCC and WMO:

The global and annual mean change in the net irradiance at the tropopause from a radiative perturbation after allowing the stratosphere temperatures to re-adjust to the radiative equilibrium, but with surface and troposphere temperatures held fixed at their unperturbed values.

Firstly, it is worth observing that this definition embodies some fundamental thermal properties of both the earth-troposphere-system and the stratosphere. When perturbing the concentration of a radiatively active atmospheric component (i.e one or more greenhouse gases), this gives rise to an immediate change in the irradiance at any vertical level affected directly or indirectly by the perturbation. Although such a 'snapshot' of the change

in irradiance (referred to as the *Instantaneous forcing*) may provide a fair a priori estimate of the warming or cooling potential of the gaseous species in question, it is inaccurate in the sense that it does not incorporate the long-term radiative effects of the perturbation. From the definition of heating and cooling rates, we know that the temporal change in temperature in a given vertical layer is proportional to the local change in irradiance. In other words, a vertical slab whose radiative balance is perturbed will ultimately seek to establish a new equilibrium temperature. However, the period of time over which this temperature readjustment takes place differs significantly from the troposphere to the stratosphere. Whereas the stratosphere typically reaches its new equilibrium in the course of a few months, the surface-troposphere system may need several decades to readjust thermally. In this way, the above definition of radiative forcing incorporates the stratospheric temperature change as a part of the forcing itself, thus establishing the tropopause as the obvious vertical level at which the forcing should be measured. The marked difference in readjustment time between the troposphere and the stratosphere also justifies the convention of keeping the troposphere temperatures fixed while carrying out the adjustment calculation.

2.5 Single profile runs - model validation

This section deals with initial runs carried out in order to validate the models' abilities to provide output in agreement with results on SWV forcings already established by others. For this purpose, we use single-profile versions of the already described SW and LW models, i.e a column of vertical layers above one single grid square. We start out with a global water vapor profile with a total of 19 vertical layers, and fix the concentration of water vapor at 6 ppmv in all stratospheric layers. This concentration is subsequently perturbed by 0.7 ppmv and radiative forcings at the tropopause pressure level (100.5mb) is studied. This water vapor profile has been used in a number of papers, most notably in Forster et al. (2001) and Zhong and Haigh (2003), and is thus a natural choice in terms of producing consistent comparisons .

As a second test of the models, we use the same SWV perturbation scheme, but applied to a typical midlatitude summer profile of water vapor. This profile, with its 33 layers, has a higher vertical resolution and is compared to a line-by-line code using the discrete ordinate method of Stamnes et al. (1988) to calculate fluxes. This second comparison allows us to study the eventual importance of using more vertical layers, as well as differences arising from the choice of water vapor profile.

2.5.1 SW validation

Comparison of SW single profile with published results

Table 2.1 shows shortwave radiative forcings obtained by several researchers using the global water vapor profile. The solar zenith angle is in all cases equal to 30°. We see that our SW single profile model is generally in good agreement with recent published results. Deviations between our estimate

Type	Reference	Forcing
LBL	Zhong et al. (2001a)	-0.102 W/m^2
k-dist	Zhong and Haigh (2003)	-0.101 W/m^2
Two-stream	Zhong and Haigh (2003)	-0.105 W/m^2
Two-stream	Ewards and Slingo (1996)	-0.054 W/m^2
Single prof.	This thesis	-0.094 W/m^2

Table 2.1: Single profile SW-model compared to published results using global WV-profile

and the others listed in Table 2.1 lie between 2-10%. The value obtained by Ewards and Slingo (1996) is likely to be an underestimate, as is also pointed out in the paper.

Comparison of SW single profile with line-by-line code:

	LBL	Our SW
Instantaneous forcing at 179 hPa	-0.116 W/m^2	-0.118 W/m^2

Table 2.2: Single profile SW-model compared to lbl using midlatitude summer WV-profile

When applying the midlatitude summer profile with a zenith angle of 30° and 33 vertical levels, we obtain a forcing at 179 hPa at -0.118 W/m^2 using the same uniform 6 ppmv to 6.7 ppmv perturbation of water vapor, now in all levels above 179 hPa. This is very close to the -0.116 W/m^2 calculated by use of a line-by-line model , once again indicating that our broadband SW model is capable of correctly representing the effect of increased water vapor in the uppermost levels of the model.

2.5.2 LW validation

Type	Reference	Forcing at 150 hPa
Corr. k-dist	Oinas et al. (2001)	0.26 W/m^2
LBL	Forster and Shine (2002)	0.28 W/m^2
NBM	Forster and Shine (2002)	0.29 W/m^2
OBIR Single prof.	This thesis	0.28 W/m^2

Table 2.3: Single profile LW-model compared to published results using global WV-profile

Comparison of LW single profile with published results
For the LW validation we once again apply the global water vapor profile used in Forster and Shine (2002). Water vapor levels are now perturbed from 6 ppmv to 6.7 ppmv at pressures lower than 150 hPa. We look at the resulting forcing at 150 hPa as a means of comparing our model output to

results obtained by other researchers. Altogether, we see that our LW test run results show good agreement with other radiation codes, indicating that our model is capable of properly representing the radiative transfer associated with the applied SWV perturbation.

Comparison of LW single profile with line-by-line code:

	LBL	Our SW
Instantaneous forcing at 179 hPa	0.317 W/m^2	0.324 W/m^2

Table 2.4: Single profile LW-model compared to lbl using midlatitude summer WV-profile

As a final test, we once again use the midlatitude summer profile, and perturb by 0.7 ppmv above 179 hPa. This gives a radiative forcing of 0.324 W/m^2, which is in very good agreement with the 0.317 W/m^2 obtained by using a line-by-line code.

Chapter 3

Model results

This chapter is divided into three distinct, but nonetheless interconnected sections. First, the previously described idealized perturbation is incorporated into the full T21L60 SW and LW codes, and the arising radiative forcings are analyzed in detail, with a special emphasis on the mechanisms behind the modeled stratospheric temperature changes. Throughout the two subsequent sections, the primary objective is to come up with estimates of the radiative forcings from anthropogenic increases in SWV. First, we look at SWV emissions associated with scenarios for future air traffic, and estimate the radiative forcing from these prescribed emissions. Finally, we look at another human source of SWV, i.e the oxidation of anthropogenic methane. We use two different approaches to come up with plausible changes in SWV from methane-oxidation from preindustrial times to present day: One method is based on the use of available methane measurements from the HALOE-instrument, and the other uses output from a CTM of water vapor generated from modeled methane changes over the same period of time. Radiative forcings are calculated both from the two datasets used separately, and from model runs using water vapor fields constructed as a combination of the two. .

3.1 Forcing from idealized SWV perturbations

As in the previous section, our study is based upon a perturbation of the stratospheric water vapor concentration from a prescribed background value of 6 ppmv by 0.7ppmv in all layers above the local tropopause. We will now use full horizontal and vertical resolution (T21L60) and carry out model runs both in the SW and LW spectral areas. We apply longitudinally varying tropopause levels, calculated from NCEP tropopause pressure data. The increase in water vapor in this experimental setup is thought to be roughly representative of the change in SWV over the period 1979-1997. However, as pointed out in e.g Forster and Shine (2002), this is likely to be an underestimate of the true forcing for two reasons:

- Trends in SWV calculated near the tropopause are uncertain, but are possibly larger than the mean trend of 0.04 ppmv/year assumed here. As the lower stratosphere is highly climatically sensitive, this could imply an underestimate from the setup used.

- A background value of 6 ppmv is somewhat higher than estimated present-day values of around 4-6 ppmv.Forster and Shine (2002) showed that adding 0.7 ppmv to a more realistic background value increased the forcing by 14%.

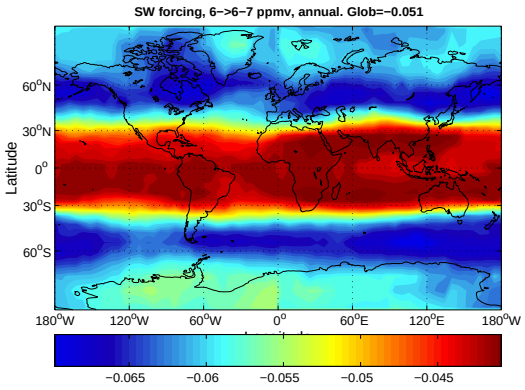

(a) SW Inst forcing, -0.051 W/m^2

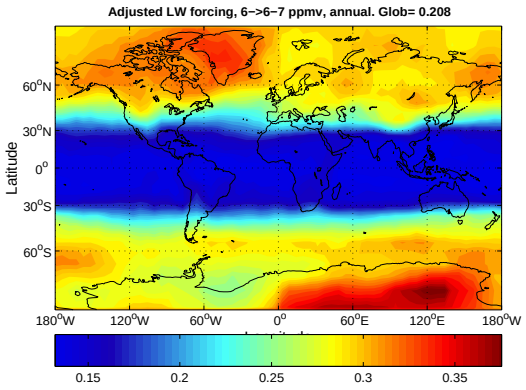

(b) Adjusted LW forcing, 0.208 W/m^2

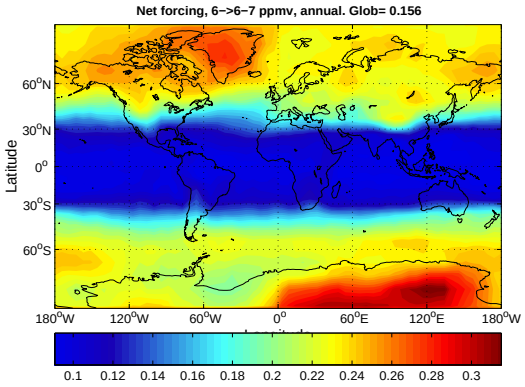

(c) Net forcing, 0.156 W/m^2

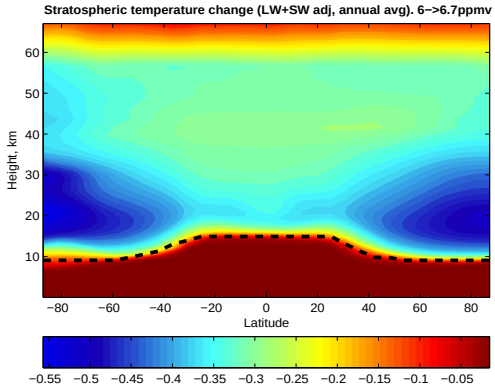

(d) Stratospheric dtemp, K

Figure 3.1: Summary of results, 6 ppmv to 6.7 ppmv SWV perturbation

Figure 3.1 summarizes the main results obtained from applying the described perturbation, i.e the various radiative responses to increasing the SWV levels from 6 ppmv to 6.7 ppmv. In Figure 3.1 a) is shown the change in SW flux at the local tropopause as computed by means of our shortwave radiative transfer model. As we can see, the obtained forcing is everywhere negative, with a global average of -0.051 W/m^2. The general sign of the forcing reflects the fact that water vapor is an absorber of SW radiation. As a consequence, the flux of SW radiation from the sun reaching the tropopause is reduced when the amount of water vapor in the stratosphere increases. Since a local rather than a global, fixed tropopause level is used in all model runs, the radiative forcing is generally evaluated at higher vertical levels on low latitudes. Thus, the perturbation from 6 ppmv to 6.7 ppmv will be applied to more vertical layers on high latitudes than in the tropics, resulting in a higher vertical "column" of added water vapor in these areas. As is

clearly seen in a), this yields a more pronounced negative forcing on middle and high latitudes than in the tropics.

In Figure 3.1 b), we find the *adjusted long-wave forcing*. As described in section 2.5, this is a measure of the change in LW irradiance following the thermal readjustment of the stratosphere after the perturbation from 6 ppmv to 6.7 ppmv. The effect of SW radiation is also included, since the extra absorption of SW radiation serves to warm the stratosphere slightly, thereby contributing to the adjusted LW forcing. As we can see, this forcing is positive, with a global average of 0.208 W/m^2. This is mainly due to the increased emission from the added SWV in the thermal IR spectral area, leading to an increase in downward irradiance at the tropopause. Analogous to Figure 3.1 a),we see that the forcing increases with latitude, once again reflecting the role of the local tropopause height.

In terms of radiative forcing in the sense defined in section 2.5, we obtain a globally and annually averaged net forcing of 0.16 W/m^2. (Figure 3.1 c)) This value is comparable to the estimate of 0.19 W/m^2 presented earlier by Forster and Shine (1999) by means of an experimental setup closely resembling ours. As emphasized in e.g Forster and Shine (2002), deviations in the forcings obtained by various researchers following such a 0.7 ppmv perturbation of SWV are likely to be caused by slight differences in the perturbation scheme and model input data rather than differences in the applied models as such. For instance, differences in choice of tropopause height, tropopause variations (global versus local) and input data (analyses versus CTM model output) have been shown to be the most likely causes of forcing discrepancies.

As for the stratospheric temperature response shown in Figure 3.1 d), we see that the imposed increase in SWV leads to an overall cooling of the stratosphere, with the greatest negative temperature changes found on high latitudes in both hemispheres. Since water vapor emits radiation in the thermal IR spectral area, an increase in concentration will lead to increased emittance of LW radiation from all vertical layers, which induces a general cooling. In addition, the added water vapor molecules also serve to absorb more of the upwelling IR radiation originating from the upper tropospheric layers, reducing the incoming IR flux in all layers except for in the lowermost stratospheric layer, where the incoming flux from below is unaffected by above changes in SWV. This effect is thought to be somewhat less important than increased emission in terms of its effect on temperature, but may still serve as an explanation for the weaker cooling directly above the tropopause.

Regarding the bimodal pattern of the temperature change, showing a less pronounced cooling in the lower tropical stratosphere, the main explanation lies in the atmospheric temperature profile. The cold point in the tropical tropopause allows for a greater incoming flux into this region, since warmer layers are situated both below and above, limiting the relative importance of the locally increased emission from the added water vapor.

Finally, it should be noted that the modeled stratospheric coolings also play an important role in terms of radiative forcings since a general decrease in temperature is equivalent to everywhere lower emissions of thermal IR radiation. Thus, the instantaneous forcing in this case, i.e the change in IR irradiance before reaching a new thermal equilibrium, was found to be

significantly larger with a value of 0.27 W/m^2 (not shown).

Radiosonde and satellite temperature data from WMO show that the midlatitude lower stratosphere has cooled by between 0.75K and 1.5K over the period from 1979 to 1994 (Shine et al. (2003),WMO (1998)). This observed cooling is even more pronounced in the lower polar stratosphere, where coolings trends of up to 5K/decade are found by Graf et al. (1998) in the winter and springtime over the period 1979-1997. This phenomenon is generally thought to be a consequence of a combination of stratospheric ozone loss as well as increased concentrations of well-mixed greenhouse gases and stratospheric water vapor.

As we can see from figure 3.1 d), our imposed water vapor change gives rise to stratospheric coolings of up to 0.55K on high latitudes in the lower stratosphere, with values of between 0.3K and 0.4K on midlatitudes and in the tropics. As emphasized in Shine et al. (2003), our idealized perturbation setup is rather unreliable in terms of giving a realistic estimate of the actual temperature change having taken place as a consequence of SWV increases over the period (1979-1997). This is mainly due to the dependence of results on the background value of SWV, which in our case is somewhat unrealistic both in terms of vertical distribution and magnitude. Therefore, the modeled temperature response does not justify any further conclusions at this point regarding the impact of SWV on the overall observed stratospheric temperature trends. However, it shows good agreement with the stratospheric temperature response modeled by e.g Forster and Shine (2002) using the same imposed WV perturbation.

3.1.1 Single-layer water vapor perturbations and stratospheric temperature changes

Regardless of the shortcomings of the modeled temperature response in terms of realism, it may still serve as a good basis for investigating some of the more detailed aspects of stratospheric cooling by WV changes. Thus, to further improve our understanding, we have carried out four test runs involving stratospheric temperature adjustment. These are all based on changing the amount of WV in specifically chosen single layers of the stratosphere. We have picked out the 1st, the 5th, the 10th and the 15th layer above the local tropopause, and model runs are performed after perturbing the water vapor from 6 ppmv to 6.7 ppmv in one of these layers at a time, leading to four different patterns of stratospheric temperature response (the effect of SW flux changes is not included in this discussion). This gives us the opportunity to study the temperature response of water vapor changes in specific layers, thus improving our understanding of the overall field in Figure 3.1 d).

When analyzing stratospheric temperature responses in general, the expressions for IR heating and cooling rates are essential in terms of explaining the modeled temperatures. The latter are in fact nothing more than a "tracer" of the changes in vertical fluxes that have taken place as a result of some perturbation of one or more atmospheric species. Thus, in these particular four cases, as in any other such setting, we need to assess in detail the flux changes having taken place in order to tie these directly to the temperature response in question. This defines our first task: identifying the

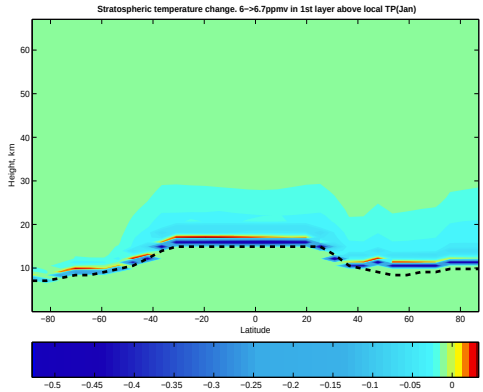

(a)WV perturbed in 1st layer above local TP

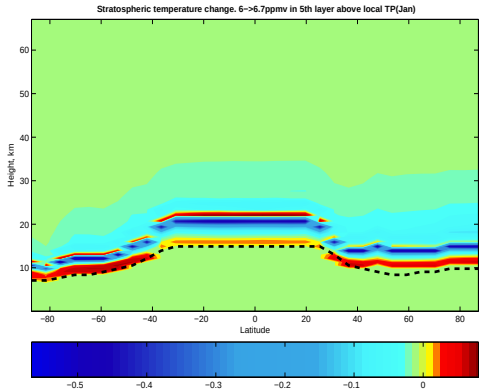

(b)WV perturbed in 5th layer above local TP

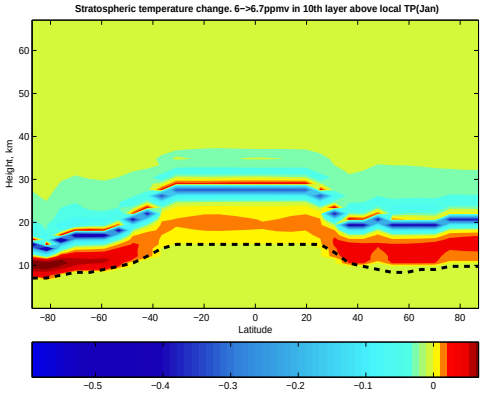

(c) WV perturbed in 10th layer above local TP

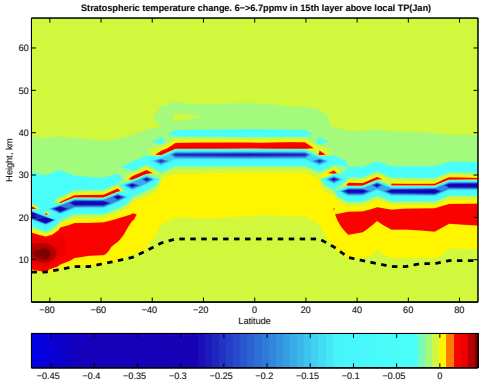

(d) WV perturbed in 15th layer above local TP

Figure 3.2: Stratospheric temperature response after WV perturbation in different single vertical layers

fluxes present in our scenarios and their degrees of change after the applied WV change. From the theory of atmospheric radiative transfer, we know that any vertical slab absorbs and emits radiation in the IR. Thus, changes in the flux entering or leaving a layer come as a result of either a change in emittance from the layer or in altered incoming irradiance from neighboring or distant layers, increasing the layer's absorption.

When looking at the temperature responses depicted in Figure 3.2 we immediately recognize one common feature, namely a band of cooling stretching across the entire latitudinal domain. This is in fact the layer to which we have applied the WV perturbation in the different cases. When adding water water vapor locally in a layer, the emittance of LW radiation increases both upwards and downwards, leading to an increase in the flux leaving the layer. This corresponds to a lowered local temperature, as can easily be seen from the definition of IR cooling rates (eq. 2.14). However, the added water vapor will also absorb more of the radiation originating from below and above layers (the latter is less important) than was the case before the perturbation. Looking once again at the IR heating rate expression, we see that this effect in the isolated sense serves to warm the layer. The radiation entering

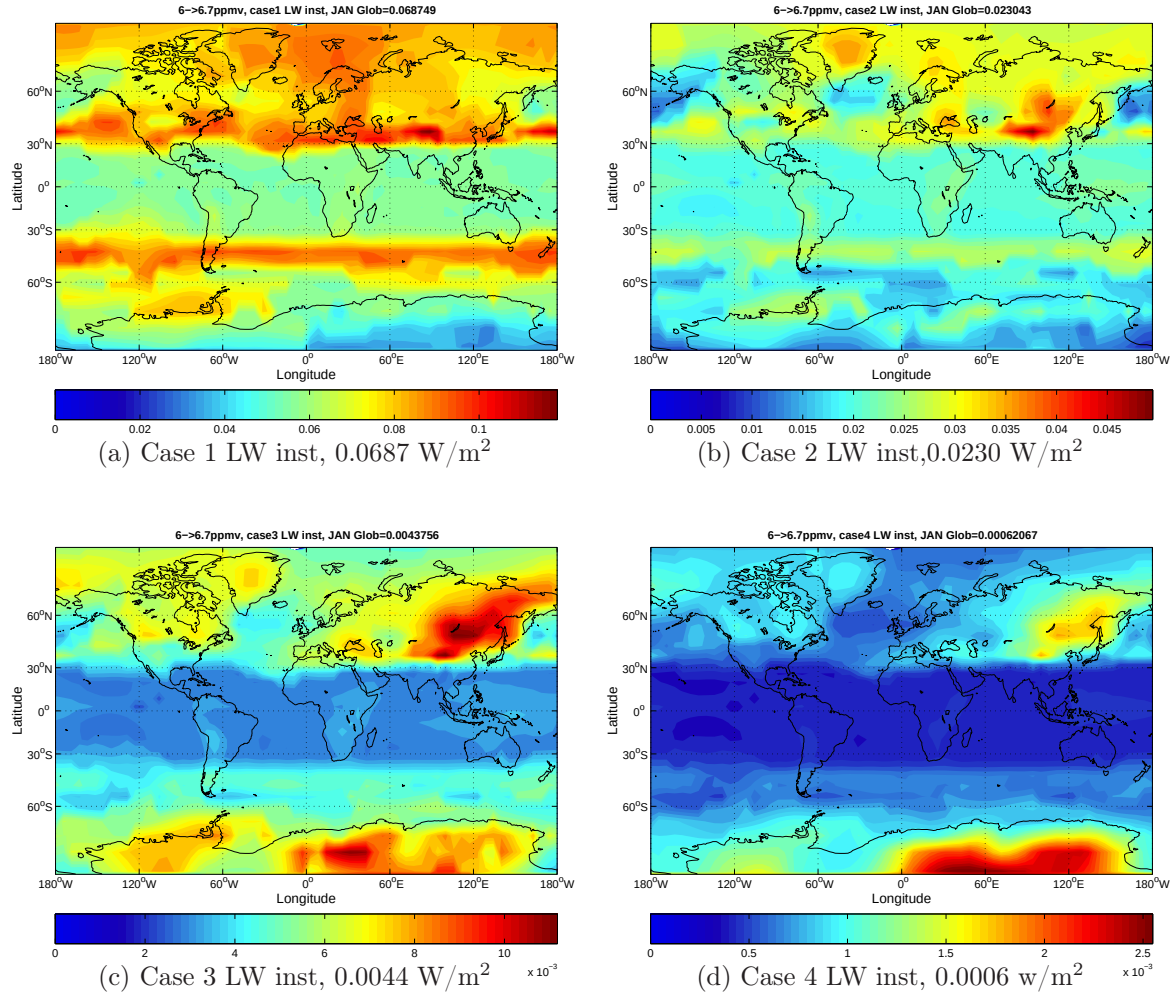

(a) Case 1 LW inst, 0.0687 W/m^2

(b) Case 2 LW inst,0.0230 W/m^2

(c) Case 3 LW inst, 0.0044 W/m^2

(d) Case 4 LW inst, 0.0006 w/m^2

Figure 3.3: Sensitivity test cases, 6 ppmv to 6.7 ppmv instantaneous forcing

the layer from below can be seen as a remnant of the terrestrial infrared blackbody radiation emitted from the surface of the earth. However, due to the greenhouse properties of water vapor (and other gases), the majority of the radiation originating from the surface has already been absorbed in lower layers. Thus, the radiation entering the perturbed layer from below originates largely from the cold upper troposphere, thereby diminishing its importance in terms of being able to heat the layer through absorption. Thus, the net result is a cooling of the layer, since emission is locally more important then absorption.

A second and equally important characteristic of the fields b)-d) is the warmer band between the perturbed layer and the tropopause. This is where the radiation emitted from the layer is absorbed, thereby causing a warming. As is evident, the vertical extent of this heated region increases as the perturbed layer is moved upwards, although the maximum magnitude of the temperature increase is rather constant throughout the cases. As can also be seen from the Figures, a second band of warming is situated directly above the lower cooling band. This response is somewhat less trivial to explain, and can be considered as an atmospheric response following the

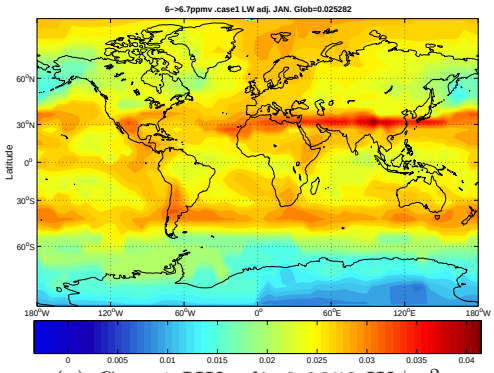

(a) Case 1 LW adj, 0.0253 W/m^2

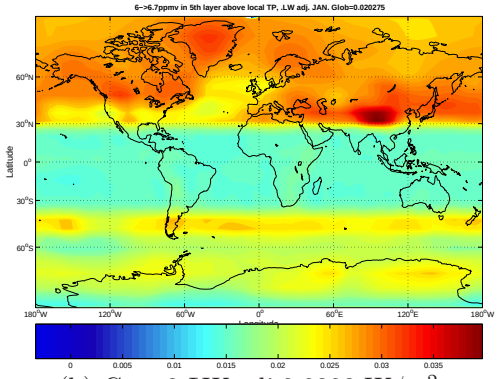

(b) Case 2 LW adj,0.0203 W/m^2

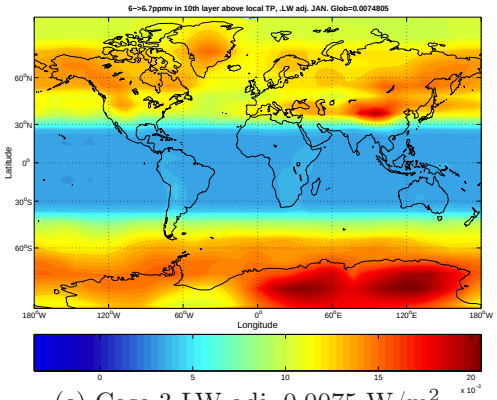

(c) Case 3 LW adj, 0.0075 W/m^2

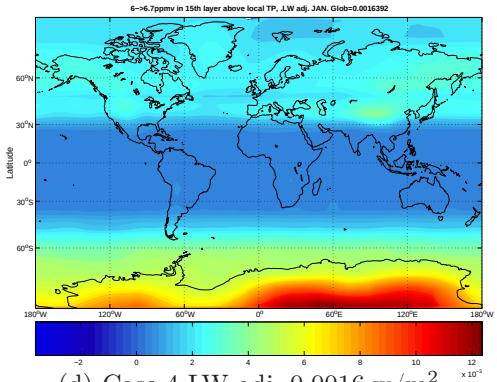

(d) Case 4 LW adj, 0.0016 w/m^2

Figure 3.4: Sensitivity test cases, 6 ppmv to 6.7 ppmv adjusted forcing

cooling produced by the extra water vapor. The modeled heating rises the obvious question of why one does not see a warming of especially the lower stratosphere when perturbing the water vapor in all layers, as done in Figure 3.1 d). The key to answering this question lies in the fact that the coolings in the perturbed layers are roughly an order of magnitude greater than the lower stratospheric warmings, thus indicating that when perturbing all layers, any modeled heating from higher layers is "overridden" by the heat loss generated by the locally increased water vapor. In this context, Figure 3.2 a) further strengthens this idea, since the water vapor added in the lowermost stratospheric layer causes re-emission downwards into the troposphere rather than to the stratosphere, thus producing a heat loss rather than a heat gain in the lowermost layer. Thus, in a sense, the lowermost layers prevent any lower stratospheric warming from taking place in the case of perturbations in all layers, as is verified by Figure 3.1 d).

Finally, Figures 3.3 and 3.4 show, respectively, the instantaneous and LW adjusted radiative forcings connected to the described single layer perturbations of SWV. In both of the first two cases, the stratospheric adjustment leads to a significant (in the relative sense) negative change in irradiance. This reflects the dominance of the lowermost stratospheric layers in terms of affecting the overall forcing. Turning to Figure 3.3 c)-d) and Figure 3.4 c)-d)

we notice that the adjustment now causes the forcing to increase. As can be seen from the corresponding temperature fields in 3.2, the layer of cooling has now moved farther away from the local tropopause, thus increasing the relative importance of the modeled heating in the more climatically significant lower layers. A further manifestation of the leading role of the coolings in lower layers is also evident when looking at the magnitudes of the forcings themselves, showing a decrease of two to three orders of magnitude when moving the perturbation from the 1st to the 15th stratospheric layer.

3.1.2 The impact of tropospheric water vapor on stratospheric temperatures

In order to complete the discussion of water vapor and temperature changes, one final investigation seems natural at this point: Until now, we have restricted ourselves to manipulating water vapor concentrations in the stratosphere. However, as was seen in the previous subsection, the tropospheric water vapor also plays a role in the stratospheric temperature adjustment process through the blocking of fluxes originating from lower levels. In order to improve our understanding of this particular phenomenon, the following experimental setup was implemented and run for one month (January):

- Reference: No tropospheric water vapor. All stratospheric WV set to 6 ppmv.
- Perturbation: No tropospheric water vapor. All stratospheric WV perturbed to 6.7 ppmv.

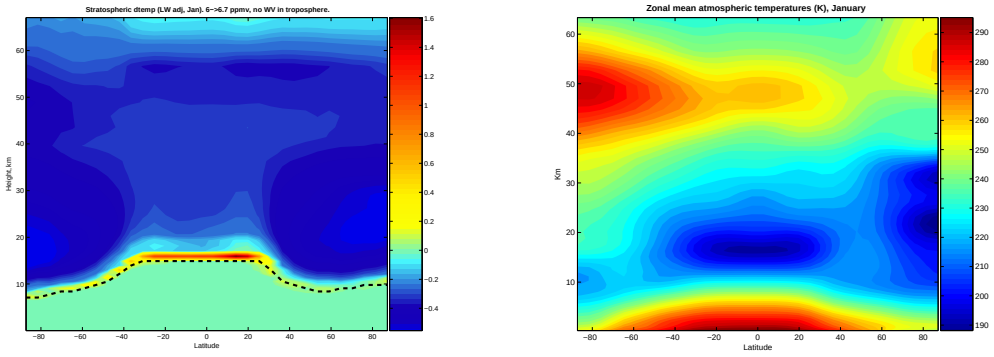

(a) Stratospheric temperature response (b) Zonal mean temperatures, Jan. (ECMWF)

Figure 3.5: Modeled temperature response and zonally averaged analysis temperatures,ECMWF (Jan)

The stratospheric temperature response following this run is seen in Figure 3.5. The most notable difference from Figure 3.1 d) is found in the lowermost stratospheric layers, where we find a generally positive temperature change with a marked peak in the tropics. This pattern of warming arises from several reasons: Firstly, the heating due to radiative exchange with surface and near-surface layers increases, as radiation originating from these

levels is able to penetrate into higher levels in the absence of tropospheric water vapor. This may partly serve as an explanation for the generally positive temperature change taking place immediately above the local tropopause. Secondly, the significantly stronger warming above the tropical tropopause is a direct consequence of the marked temperature minimum found in this area, as shown in Figure 3.5 b). In regions such as the troposphere, the temperature falls of with height in a relatively linear fashion. Thus, the heat exchanged between a vertical layer and neighboring higher-altitude layers will be largely offset by interaction with lower neighboring layers. In the tropical tropopause, however, radiation arrives both from the warmer stratosphere and from the warmer troposphere. As we have already established, the amount of incoming radiation from the troposphere increases significantly when removing tropospheric water vapor, paving the way for an net increase in incoming radiation that forcibly is at a maximum in the tropical tropopause due to this enhancement by temperature conditions.

When moving away from the tropopause, the temperature response begin to resemble that depicted in Figure 3.1 d). Since the temperature profile is once again linear with height, the net exchange between neighboring layers decreases. Also, the absorption of the extra upwelling radiation quickly reaches its peak, further diminishing the effect of a "transparent" troposphere. Thus, the changes in radiative transfer is increasingly dominated by the change in SWV content from 6 ppmv to 6.7 ppmv, lowering the temperature by increased emission, as already seen in the previous section.

3.2 Radiative impact of future aircraft emissions

As previously stated, increased concentrations of SWV are thought to have arisen partly as a direct consequence of human activity and partly as a feedback from changes in the climate system. An investigation of the latter is a topic of current research, and lies well beyond the scope of this thesis. However, quantifying the anthropogenic component of the SWV increase is no less important, since any radiative impact of such a human contribution can be considered as a direct climatic forcing. An obvious anthropogenic candidate for increases in SWV is the emission of water vapor from civil air traffic, which has increased sharply in the past 50 years, and is likely to continue doing so in the future.

3.2.1 Scenario descriptions

Major European airframe companies have announced intentions to develop a supersonic aircraft for use in future commercial air traffic. This has raised concerns in terms of the possible environmental impact, and in IPCC (1999b), an attempt was made to quantify the effect of gases and particles from future sub- and supersonic aviation. However, the conclusions presented by IPCC had large uncertainties, and a call for further research was made. The climatic and environmental issues connected with future air traffic has since then been pursued in the EU-project SCENIC.(SCENIC (2005)).

One case was developed for the year 2025, where air traffic and fleet composition can be foreseen to a certain extent, and another for 2050, where only

a projection can be made. For each year, one scenario provides 3D emissions from a purely subsonic fleet and another provides emissions form a mixed fleet consisting of both subsonic and supersonic air traffic. This gives a total of four different scenarios. In the case of subsonic traffic only, Airbus performance files have been used in SCENIC (2005) to calculate flight profiles and fuel consumption. Emission indices(EI) (of unit [grams emitted/kg of kerosene burnt]) for various species are calculated from data available for the types of engines considered in use in the two different years. To generate realistic 3D emission fields, a number of assumptions were made regarding future flight corridors, fuel efficiency, future development of emission reduction technologies etc. This also applies to the hypothetical supersonic fleet, where emissions were calculated by selecting competitive routes for such traffic and further considering plausible marked shares based upon the need for such transport. Furthermore, supersonic traffic is also thought to introduce emissions well into the stratosphere, due to its prescribed cruising altitude at ca. 60.000 ft.

3.2.2 CTM model output

During the SCENIC project, the prescribed emissions for the four scenarios were used as input to the Oslo CTM-2 model, using T21L40 resolution. Background climatology was taken from IPCC scenarios for the corresponding years. Modeled transport and distributions for several constituents were studied, and among them was water vapor. Figure 3.5 shows the CTM-2 output for water vapor in the four scenarios. As we can see, a common feature of the zonally averaged WV fields is the restriction of the water vapor changes to the northern hemisphere, mainly north of 40°. This is nothing other than a direct consequence of the location of the world's main flight corridors. The supersonic air traffic is introduced mainly on similar latitudes as the already present subsonic traffic, but the water vapor is clearly subject to a more pronounced transport toward lower latitudes, and to some extent even into the southern hemisphere when emitted at higher vertical levels. The increase in magnitude of the water vapor change is simply a consequence of the prescribed changes in air traffic patterns with corresponding increases in fuel consumption. The increase in emissions on lower stratospheric levels between the purely subsonic and the sub- and supersonic scenarios is a consequence of restrictions applying to supersonic travel, lowering the cruise altitudes and velocity of these planes e.g over densely populated areas.

3.2.3 Radiative forcings

In order to calculate radiative forcings from these model outputs, the provided CTM data was added to the T21L40 background water vapor field (ECMWF) used as default in OBIR. The obtained longwave instantaneous radiative forcings can be seen in Figure 3.6. As is clear from the plots, the forcings from all four scenarios are small in magnitude, with the highest calculated forcing reaching as low as 0.048 W/m^2 (from the scenario "Sub+supersonic 2050"). In addition, the net forcing (as in Figure 3.1 c)) for these scenarios is unlikely to surpass the instantaneous forcing for two main reasons. Firstly, the

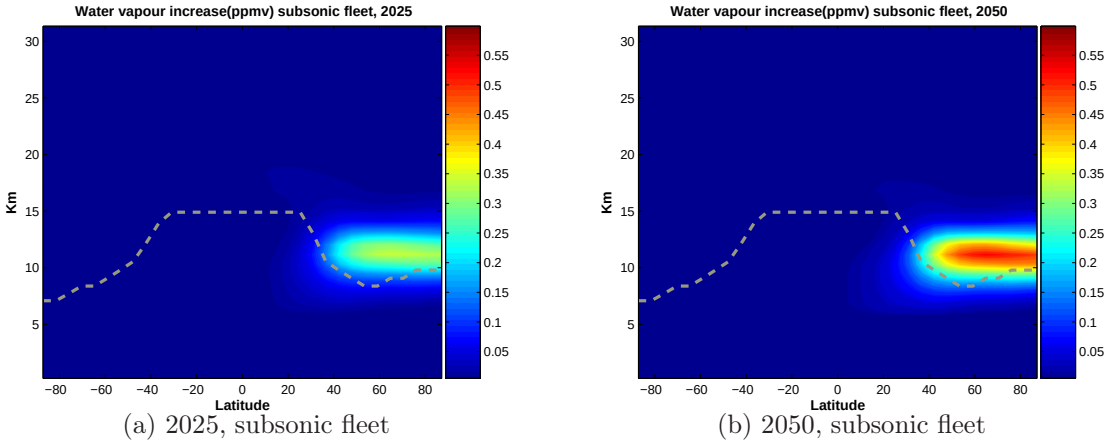

(a) 2025, subsonic fleet

(b) 2050, subsonic fleet

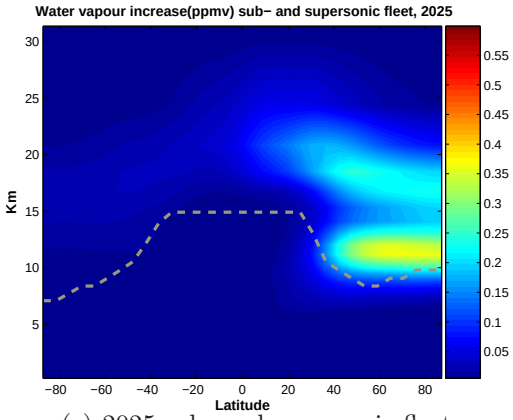

(c) 2025 sub- and supersonic fleet

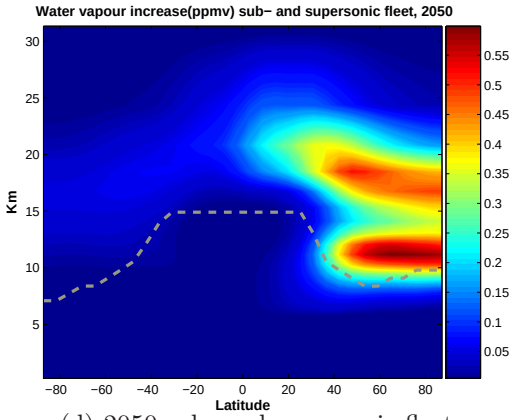

(d) 2050 sub- and supersonic fleet

Figure 3.6: Water vapor increase, aircraft emission scenarios

effect of blocked SW radiation, however small, will clearly serve to decrease the net forcing. As for stratospheric temperature responses, one may expect these to be somewhat different between the purely subsonic and the sub- and supersonic cases. In the subsonic cases, we find a fairly close resemblance in the northern hemisphere between the zonally averaged emission increases and the single layer perturbation experiment labeled as case 1 in the previous section. As was clear from this test case, an increase in SWV residing in the lowermost regions of the stratosphere, as is the case for the subsonic scenarios, will contribute to a marked cooling directly above the tropopause, thereby lowering the forcing significantly after adjustment. In the supersonic cases, an additional, but smaller increase in SWV is imposed at altitudes around 20kms. This increase, viewed separately, is comparable to the third test case of subsection 3.1.1, i.e to a narrow stratified perturbation about 10 model layers above the local tropopause. As was seen previously, a 0.7ppmv increase in this layer alone did lead to a general warming after adjustment, but one must bear in mind that its effect on the overall forcings is quite limited compared to the lower-layer perturbations. In addition, these higher-layer perturbations is no larger than 0.40-0.45 ppmv, thereby further limiting its potential for generating lower stratospheric warmings after adjustment.

Therefore we conclude, without the need for further simulations, that stratospheric water vapor originating from future air traffic as prescribed in SCENIC is only a minor contributor to the overall SWV increase when compared to increases seen over the past decades. At the same time, this is also indicates strongly that the increase in air traffic seen over the past 50 years is likely to be relatively unimportant in terms of radiative forcings. On the other hand, these emissions of water vapor may very well have a climatic impact beyond the mere radiative forcing. For instance, temperature changes originating from the added water vapor, as well as the presence of the water vapor itself may be capable of e.g affecting the general stratospheric chemistry through altering the speed or likelihood of reactions between other stratospheric species.

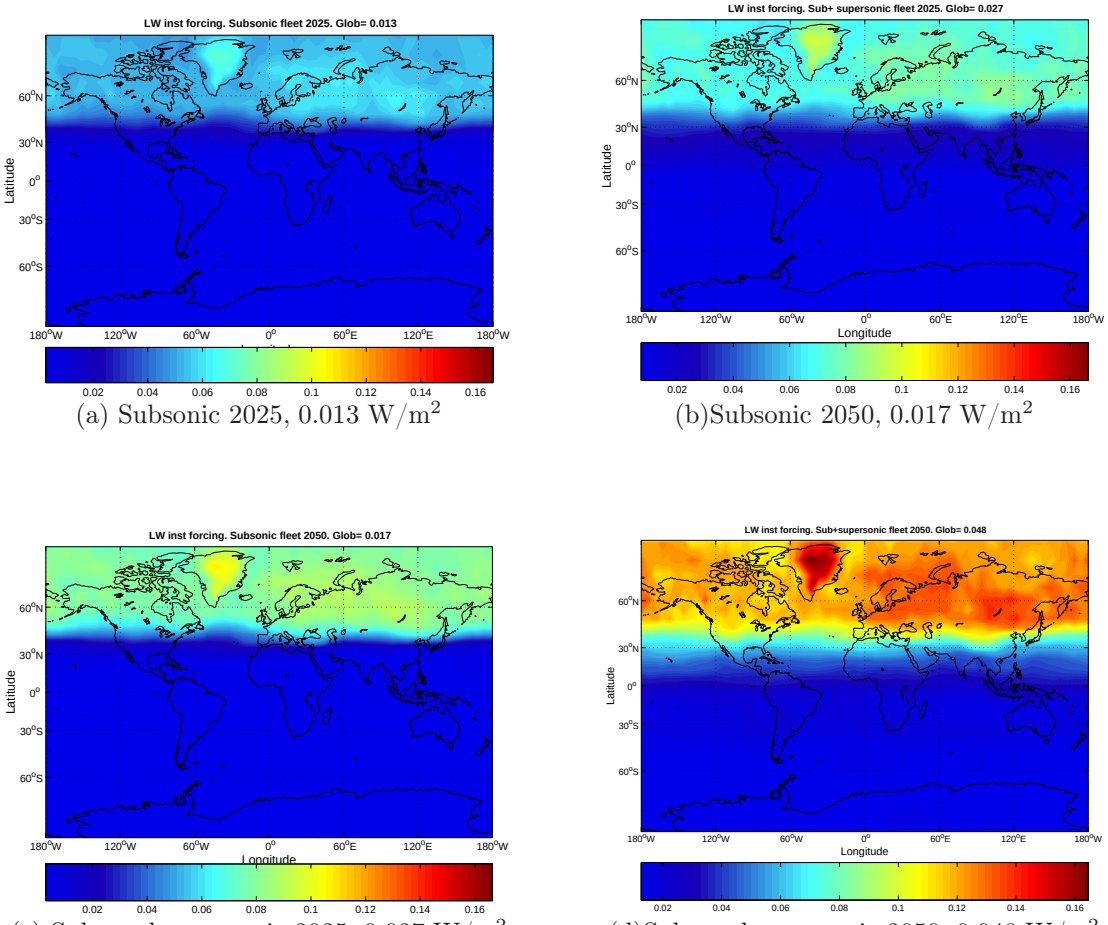

(a) Subsonic 2025, 0.013 W/m^2

(b)Subsonic 2050, 0.017 W/m^2

(c) Sub- and supersonic 2025, 0.027 W/m^2

(d)Sub- and supersonic 2050, 0.048 W/m^2

Figure 3.7: Instantaneous LW forcing from aircraft emission scenarios

3.3 Radiative forcing of SWV from methane oxidation

The primary aim of this section is to investigate in detail the amount of SWV attributable to oxidation of anthropogenic methane. In addition to SWV emissions from aircrafts, which we have found to be relatively insignificant, any radiative forcing arising from this source of SWV can be considered as a direct anthropogenic forcing. Herein lies the obvious motivation for trying to come up with an estimate of the magnitude of this forcing.

Clearly, our first task will be the generation of a plausible H_2O change field for inclusion into the grid used in the model calculations, i.e, the T21L60 resolution. This will be done via two different pathways:

- Subtracting preindustrial methane concentrations from present day (1995) CH_4-data from the HALOE-satellite.
- Incorporating into the models the H_2O output from a CTM model for the years 1850 and 2000 respectively.

Obviously, having two different methods of H_2O field generation in our arsenal serves a priori as a consistency check of the produced fields, and could also contribute to narrowing down the final forcing estimates.

3.3.1 Generation of ΔH_2O-fields

Using HALOE-data:

The main idea behind the procedure outlined in this section is based on the aforementioned oxidation of methane taking place in the stratosphere. It is well known that methane concentrations remain virtually constant up to the local tropopause, with values gradually decreasing with height through the stratosphere. The present day tropospheric volume mixing ratio of CH_4 is known to be around 1.745 ppm. We then assume that any encountered concentration below this value is a result of methane having been oxidized into H_2O, thus increasing the (stratospheric) H_2O concentration by twice the amount of methane depleted. Since our interest lies in tracking the purely anthropogenic contribution to this source of SWV, we need to disregard preindustrial methane as a contributor to this SWV source. This may be stated as follows:

$$\mu_{H_2O}^{t_{1995}}(x,y,z) - \mu_{H_2O}^{t_{1850}}(x,y,z) = 2(\mu_{ref}(x,y,z) - \mu_{CH_4}^{t_{1995}}(x,y,z)) \cdot R \tag{3.1}$$

where

$$R = \frac{\mu_{CH_4}^{t_{1995}}(x,y,0) - \mu_{CH_4}^{t_{1850}}(x,y,0)}{\mu_{CH_4}^{t_{1995}}(x,y,0)} \tag{3.2}$$

and μ is the volume mixing ratio at the grid point (x,y,z) for either CH_4 or H_2O in the year indicated by the subscript. The terms $\mu_{CH_4}^{t_{1995}}(x,y,z)$ and $\mu_{ref}(x,y,z)$ denote the methane mixing ratios supplied by HALOE and an everywhere fixed reference mixing ratio of 1.745 ppmv, respectively. Thus, the subtraction involving these two terms, multiplied by two, denotes the

total current production of stratospheric H_2O from methane oxidation. However, we need to disregard the fraction of this production that comes from oxidation of the methane that was already present at the reference time, i.e a concentration of 0.8 ppmv in the year 1850. This is done by multiplying the production term by the fraction of tropospheric methane produced by human activity, which is clearly given by the above expression for R.

We may very well apply this procedure to study the methane-induced SWV difference between 1995 and any year, as long as we insert the correct tropospheric methane concentration of the year in question. If we continue, for the time being, to use preindustrial methane values in the above expression, we may rewrite (3.2) in a more compact notation:

$$\Delta H_2O(x, y, z) = 2\Delta CH_4(x, y, z) \cdot \frac{0.945}{1.745} \tag{3.3}$$

Here we have inserted the methane volume mixing ratios for the year 1995 (1.745 ppm) and for preindustrial times (0.800 ppm). If we would like to calculate the anthropogenic change in SWV for a more recent period of time, we need only insert the CH_4 mixing ratio for the desired reference-year, yielding a smaller fraction, and hence a smaller change in water vapor concentrations.

To summarize, the results that are to be presented in this section are based on the following basic assumptions:

- The only sink of CH_4 is oxidation into H_2O.
- The concentration of methane is constant up to the local tropopause.

The forcing calculations are ultimately based on a set of zonally averaged methane data from HALOE, given as monthly means averaged over the period 1991-1999. Hence, to simplify, we denote "present-day" as 1995. The data covers latitudes from -80° to +80° with a resolution of 4°. Vertically, there are 25 global pressure levels ranging from 100 hPa to 0.01 hPa. However, the spatial coverage is not complete for all months, with "white spots" mostly confined to areas of high latitudes and low pressure values. This presents a number of challenges with respect to inclusion of the HALOE-data into the desired 3D grid, i.e T21L60:

1. Filling in "best guess" data in uncovered areas by means of some interpolation scheme.
2. Extending latitudinal coverage to from (-80°,+80°) to (-90°,+90°).
3. Vertical interpolation of HALOE-data into the model.

These operations were all carried out by use of a constructed matlab-script, and the resulting water vapor change fields for January and July are shown in Figure 3.8

Using CTM model output

Apart from the use of HALOE-data to generate H_2O change fields, we have also used the output from a CTM simulation of water vapor concentrations from 0 to 30kms on a T21 horizontal grid for the years 1850/1950

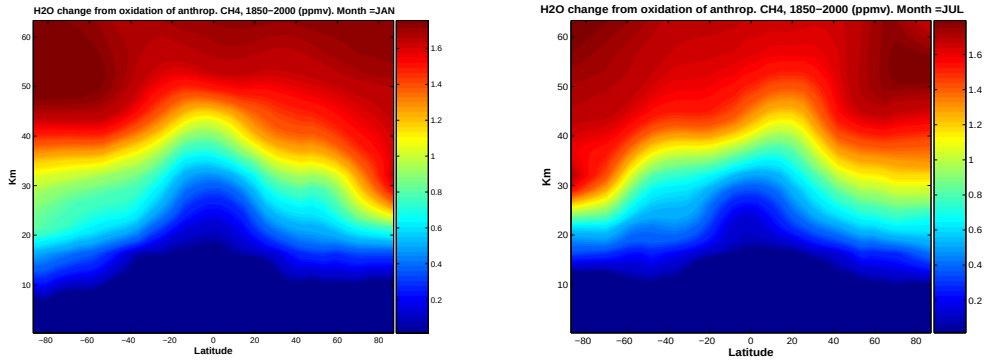

(a) January (b) July

Figure 3.8: Zonally averaged water vapor change 1850-2000, generated from HALOE data

versus the year 2000. This corresponds to using a T21L40 3-dimensional grid, as opposed to the T21L60 grid used for the HALOE-data. Thus, the vertical extent of these data is more limited than in the HALOE-case, but this may pose as much of an opportunity as a limitation, given the possibility of exploring the importance of the middle stratospheric water vapor change (30km-60km) derived from HALOE in terms of radiative forcings. The joining of the fields is done by a vertical spline interpolation of the CTM data into the T21L60 grid. At this point, with both HALOE and CTM data sets in the same grid, we now choose to incorporate the following water vapor changes into two different model runs:

- Original CTM output data only (extending vertically up to 30km) with WV change set to zero in above layers.

- A mix of CTM output data (up to 30km) and HALOE data (30km to 60km)

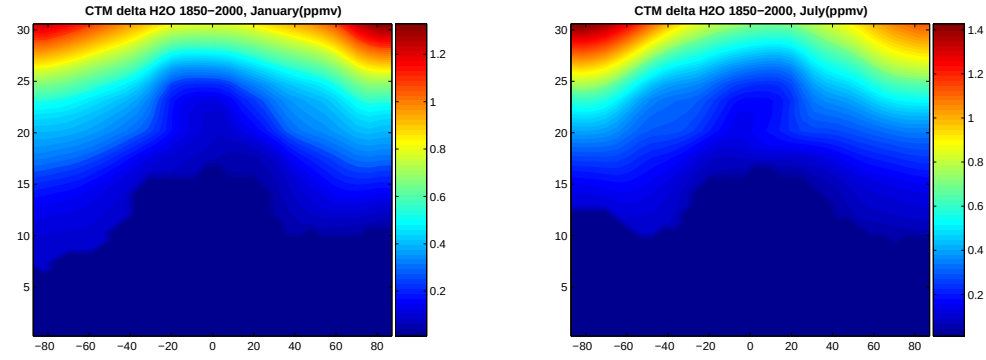

(a) January (b) July

Figure 3.9: Zonally averaged water vapor change 1850-2000, generated from CTM data

3.3.2 Radiative forcings from generated fields

Forcings from HALOE-data fields:

Once the HALOE-based field is generated, inserting it into our LW and SW models provides us with radiative forcings from oxidation of anthropogenic methane, i.e, a direct forcing on the climate. Simulations are carried out for the periods 1750-1995(not shown), 1850-1995 and 1950-1995.

Firstly, we see from Figures 3.10 a) and 3.11 a) that the SW forcing from the imposed water vapor increases is rather modest, with values of -0.018 W/m^2 and -0.011 W/m^2, respectively. Comparing with the corresponding SW flux from the uniform 0.7 ppmv-case, we may infer that water vapor added on high levels has a small impact on the change in SW irradiance at the tropopause height. In the 1850 HALOE-run, the amount of water vapor exceeds 0.7ppmv above 20km (ca.30km in the 1950-run), with lower values nearer the tropopause. Thus, it is clearly the lower-stratospheric water vapor that is crucial in determining the magnitude of the SW forcing.

The adjusted LW forcings, including the warming effects of absorption in the SW spectrum, have values 0.095 W/m^2 and 0.050 W/m^2 for the two periods. Bearing in mind the above remarks on the differences between these runs and the previous uniform-increase case, this once again reflects the importance of the lower stratosphere in terms of affecting the forcing,

The derived net forcings, both for 1850-1995 of 0.077 W/m^2 (Figure 3.10 c)) and for 1950-1995 of 0.050 W/m^2 (Figure 3.11 c)) are clearly climatically significant, confirming that a direct human forcing is taking place as a result of the methane oxidation. If we now turn to the work of Forster and Shine (2002), an estimate of the forcing from the total increase in SWV over the period 1960-2000 is given, based on all available time series of SWV measurements. In this paper, a global trend of 0.05 ppmv/year between 100 hPa and 10 hPa is imposed as representative for the entire stratosphere although it is thought to be significantly higher at pressures above 100 hPa. The resulting net forcing for the period from 1960 to 2000 is then shown to be 0.63 W/m^2 for a global trend and 0.21 W/m^2 for a trend confined to the northern hemisphere only. If we choose to compare these results with our net forcing as shown in Figure 3.11 c), our derived methane oxidation forcing may constitute between 8%and 25% of the total estimated forcing from water vapour. It must be stressed, however, that the referred trends are highly uncertain and serves as something of a "best guess" based on all available data as of today.

Turning now to Figure 3.10 d), we find an immediately interesting aspect in the temperature response field. As we can see, a band of positive temperature changes is found immediately above the local tropopause. This may seem somewhat surprising, given the much discussed link between stratospheric cooling and increased SWV. If we turn back to the four experimental cases discussed in section 3.1, we know that the layers just above the local tropopause are crucial in determining both the overall forcing as well as the sign of the temperature response in the lower stratosphere. The idealized increase of 0.7 ppmv was shown to be sufficient in terms of producing an overall cooling directly above the local tropopause, since warmings from perturbations in upper layers were overridden. When inspecting the imposed HALOE water

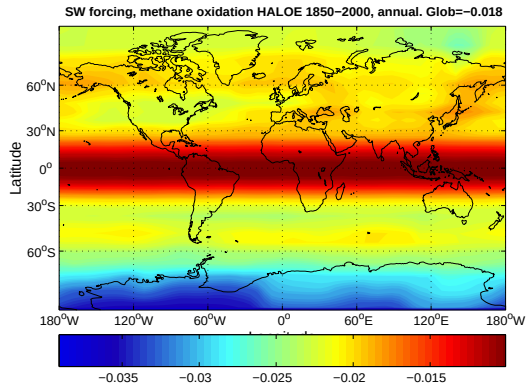

(a) SW Inst forcing, -0.018 W/m^2

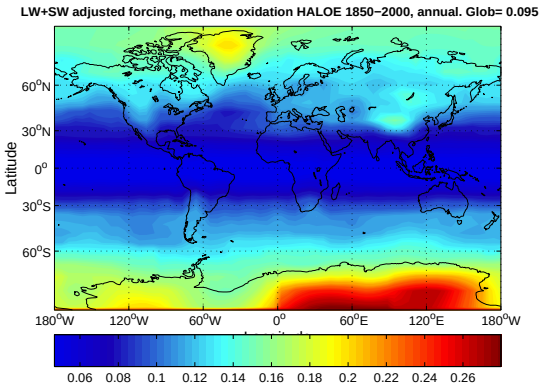

(b) Adjusted LW forcing, 0.095 W/m^2

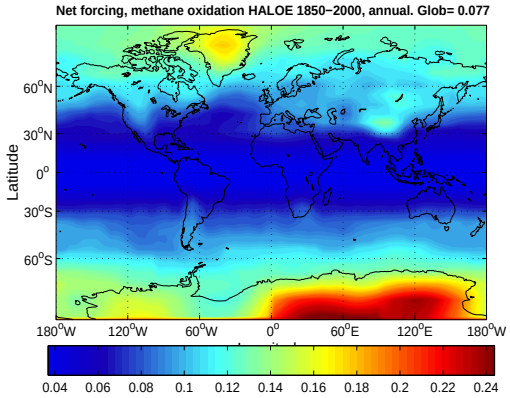

(c) Net forcing, 0.077 W/m^2

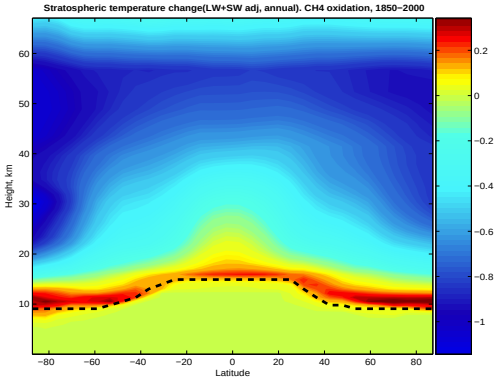

(d) Stratospheric dtemp, °K

Figure 3.10: Summary of results, methane oxidation, 1850-2000, HALOE data

vapor change fields (Figure 3.8), however, we can see that the perturbation in the lower stratosphere is significantly lower than 0.7 ppmv, and almost an order of magnitude smaller in the lowest stratospheric model layer. As pointed out in the case-discussion, the more water vapor we add to a layer, the more local cooling will be produced as a result of increased emission. Hence, when adding only small amounts of water vapor immediately above the local TP, the local cooling in these layers will be correspondingly moderate and easier to "override" by the warming effects from increases in above layers. Bearing in mind that upper stratospheric water vapor changes as modeled from the HALOE data exceed 0.7ppmv, it seems reasonable that the lower stratospheric warmings resulting from these perturbations will be significantly greater than in the case of a 0.7 ppmv increase. Thus, on the overall we may interpret the band of lower stratospheric warming in Figure 3.10 d) as a result of moderate local cooling from small lower stratospheric perturbations and a relatively high degree of lower stratospheric warming from large perturbations in higher layers.

As for the impact of the temperature response on the radiative forcings, it turns out that the adjusted forcings given in 3.10 b) and 3.11 b) are higher than their respective instantaneous forcings(not shown). This effect

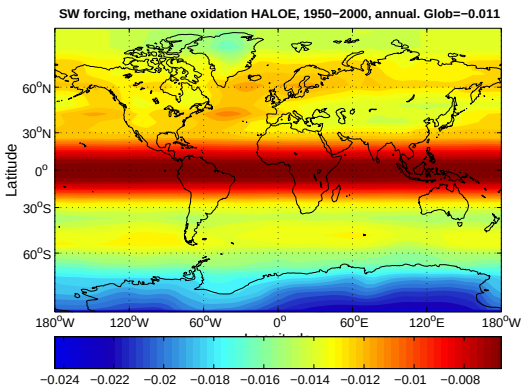

(a) SW Inst forcing, -0.011 W/m^2

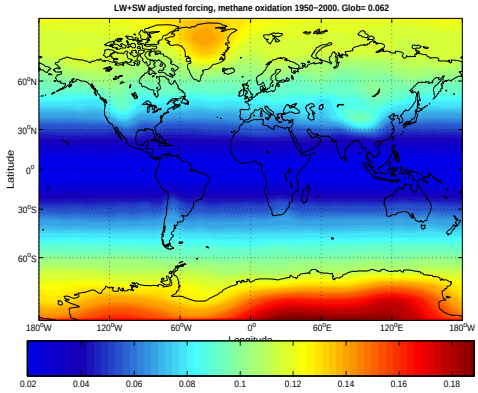

(b) Adjusted LW forcing, 0.062 W/m^2

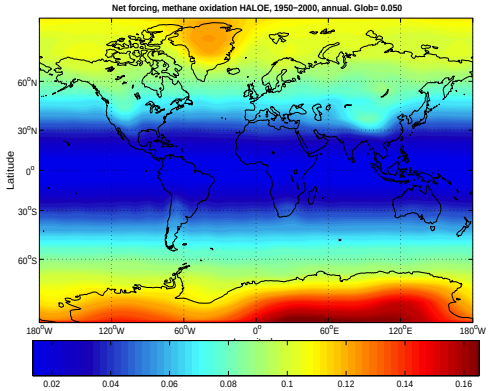

(c) Net forcing, 0.050 W/m^2

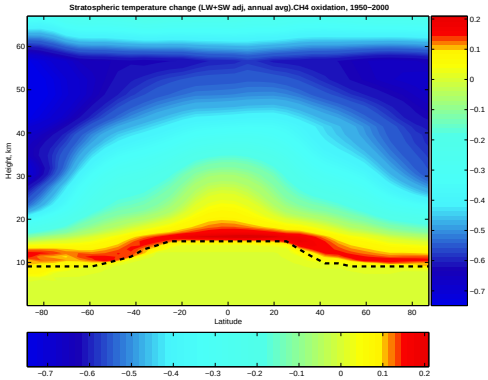

(d) Stratospheric dtemp, °K

Figure 3.11: Summary of results, methane oxidation, 1950-2000, HALOE data

was previously seen in connection with the sensitivity tests labeled as cases 3 and 4 and is depicted in Figures 3.3 c) and d) versus 3.4 c) and d) where the forcing is seen to increase substantially after adjustment. Indeed, the adjustment referred to in subsection 3.1.1 did not include shortwave effects, as is the case in these methane oxidation simulations, but this effect is still too small to alter the general picture. The instantaneous forcings were calculated to be 0.083 W/m^2 for 1750, 0.073 W/m^2 for 1850 and 0.041 W/m^2 for 1950, thus giving a relative increase in forcing after adjustment by 24% (to 0.103 W/m^2), 30% and 51%, respectively. This reflects a seemingly moderate dependence of the lower stratospheric warmings on the *magnitude* of the imposed water vapour changes, while once again emphasizing that the *vertical gradient* of the water vapour field is crucial in terms of affecting the local sign of the resulting stratopsheric temperature response.

It should be pointed out that these simulations do not in any way contradict neither modeled nor observed negative temperature trends in the lower stratosphere (e.g as presented in Shine et al. (2003)).However, they indicate that the contribution to the stratospheric temperature change from SWV changes is highly sensitive to the vertical profile of imposed lower stratospheric water vapor change.

Forcings from CTM-data fields:

The calculations on the two types of CTM-generated fields are carried out in the same way and by the same models as in the cases involving the use of HALOE-data. For the first case, i.e using of a combination of CTM-data (0-30km) and HALOE data (30-60km), we obtain forcings for the period 1850-2000 somewhat smaller in magnitude than in the case of HALOE data alone

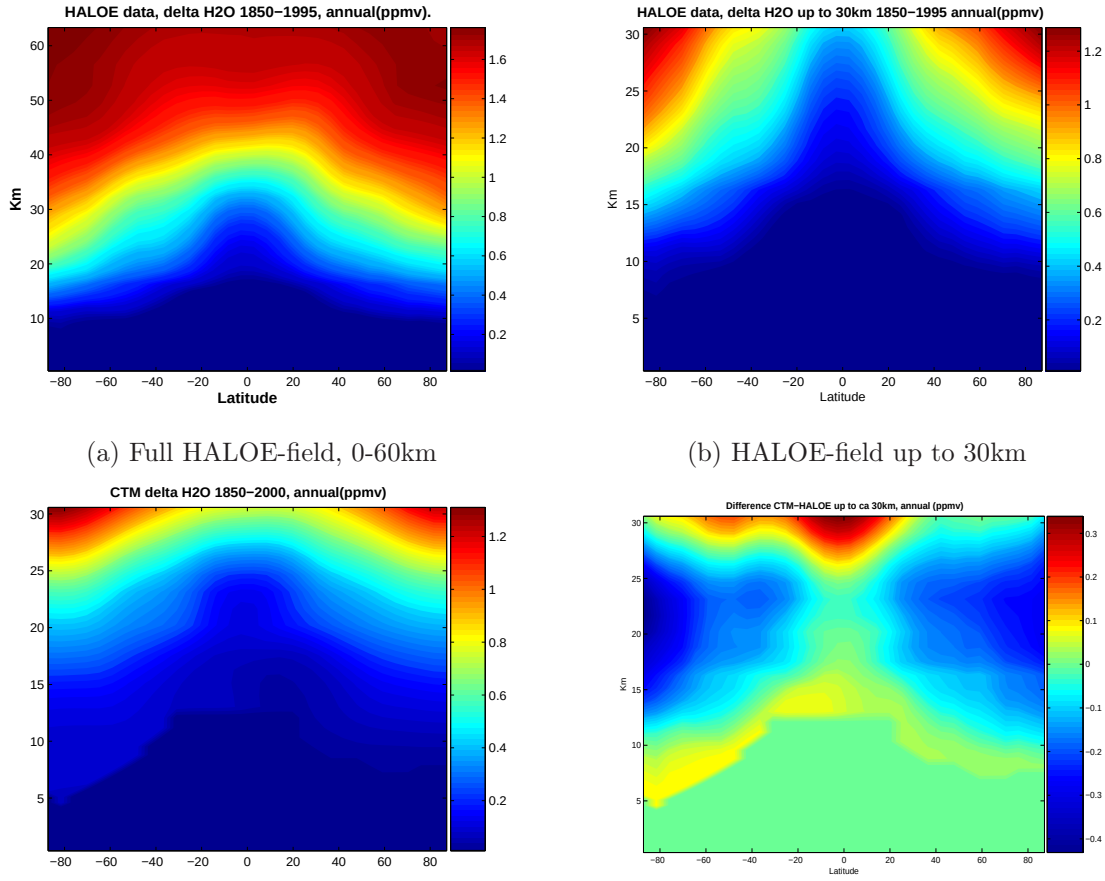

(a) Full HALOE-field, 0-60km

(b) HALOE-field up to 30km

(c) CTM field

(d) Difference between CTM and HALOE

Figure 3.12: Comparison of imposed SWV change fields. Unit is ppmv.

Generally speaking, there is fair qualitative agreement between results illustrated in Figures 3.13-3.14 and 3.10. As for the SW runs, shown in Figures 3.13 a) and 3.14 a), the forcings differ by some 25% only, despite the absence of any added water vapour above 30km in the first figure. Given the height where this difference in SWV concentration is expressed, this moderate difference between the two SW forcings once again reflect the lack of relative importance (in terms of radiation) of the high-altitude water vapor.

In addition, we once again obtain a lower stratospheric warming closely resembling that from the HALOE-perturbation. That being said, the differences in net forcings from the CTM-based experiments versus those obtained by the use of HALOE data do call for a further investigation. The obvious candidates for explaining the discrepancies are the imposed water

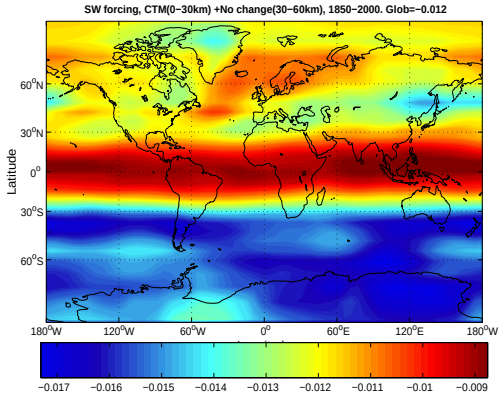

(a) SW Inst forcing, -0.012 W/m^2

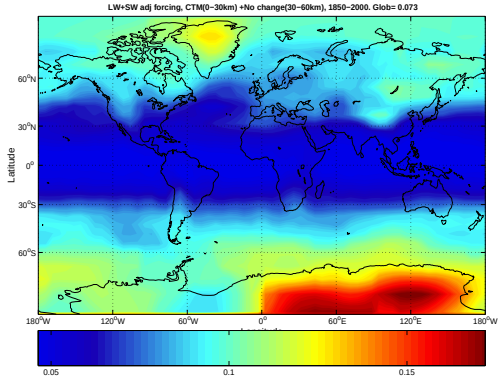

(b) Adjusted LW forcing, 0.073 W/m^2

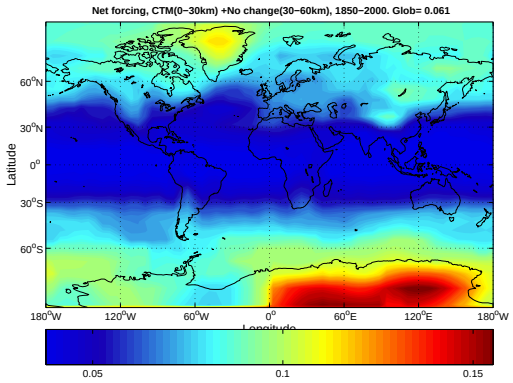

(c) Net forcing, 0.061 W/m^2

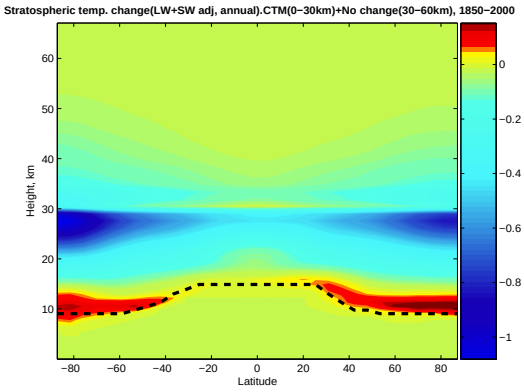

(d) Stratospheric dtemp, °K

Figure 3.13: Summary of results, CTM+no change, 1850-2000

vapor change fields, which may easily provide us with plots of the difference in added SWV between the HALOE case and the CTM cases. The region above 30km is clearly of no interest in this particular sense, thus the cutoff at 30km in the plots provided in Figure 3.12 b)-d). As we can see from Figure 3.12 d), where HALOE concentrations are subtracted from CTM concentrations, the change in SWV from HALOE is significantly greater between 15 km and 25 km on high latitudes. On the other hand, the CTM adds slightly more water vapor than HALOE in a narrow belt just above the tropopause, and significantly more at around 30kms over the tropics. This latter surplus of CTM water vapor is of less importance, due to its remote vertical location and to the high local tropopause found on these latitudes. It is worth noting that all these deviations of the CTM field from the HALOE field arise from the differences in "steepness" between the two fields, as can easily be observed from Figure 3.12 b) and c). Thus, due the fact that the HALOE-experiment seems to add significantly more water vapor in radiatively important areas of the stratosphere than does the CTM, it seems reasonable that the forcing obtained from using HALOE data turns out to be larger than the forcings from CTM-generated changes.

At this point one may be tempted to ask whether these CTM-runs provide any meaningful results at all, due to the rather large differences from the

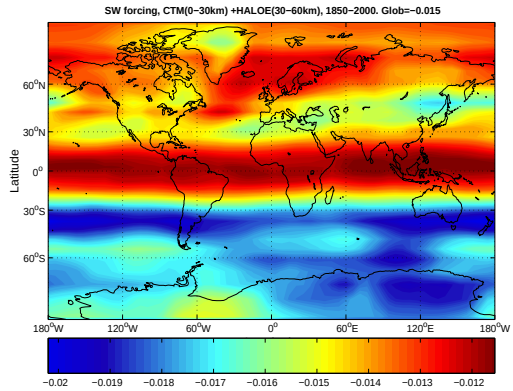

(a) SW Inst forcing, -0.015 W/m^2

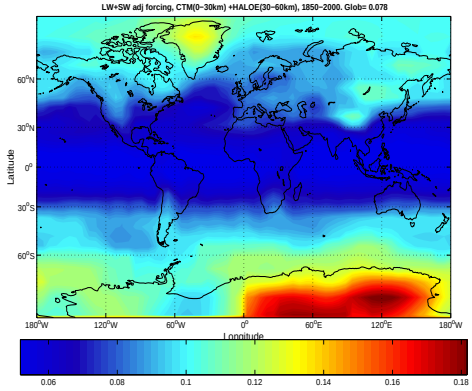

(b) Adjusted LW forcing, 0.078 W/m^2

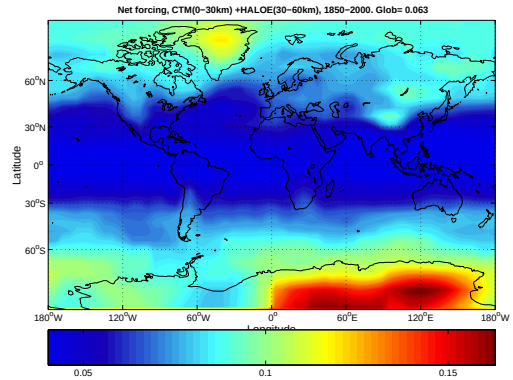

(c) Net forcing, 0.063 W/m^2

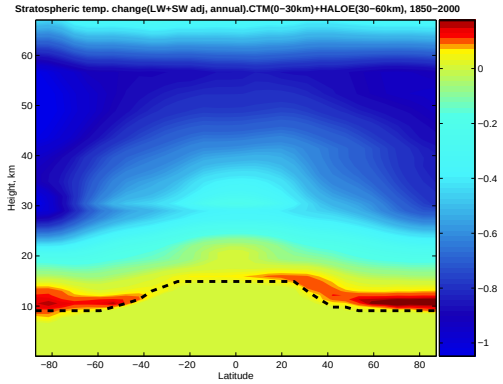

(d) Stratospheric dtemp, °K

Figure 3.14: Summary of results, CTM+HALOE, 1850-2000

previous HALOE-runs. However, although they can clearly not serve as any form of "validation" of the previous experiments due to the large differences in radiative forcings, they nonetheless embed some potentially interesting aspects. These mainly arise when one begins to compare the two different CTM runs, i.e cases with HALOE data versus no WV change for altitudes above 30km. When looking at these two runs, with results summarized in Figures 3.13 and 3.14 respectively, we first note that the difference in net forcing is no more than 0.002W/m^2. Knowing that the difference in SWV concentrations between the two runs is in the area of $\simeq$1 ppmv, this clearly shows that water vapor added above 30 km plays a very limited role in terms of net radiative forcing. However, the net forcing involves both SW and LW radiative forcing, and it is worth noting that the effect of the added SWV is somewhat larger, at least in the relative sense when looking at these two spectral areas separately. Altough the added SWV produces only a minor decrease in solar irradiance in both cases, one should note that the relative difference in forcing between Figure 3.13 a) and 3.14 a) is 25%. This shows that that water vapour added in the middle and upper stratosphere interacts more strongly with radiation in the SW spectral region. Turning to the longwave adjusted forcing shown in Figures 3.13 b) and 3.14 b), we find the difference in forcing to be somewhat limited, both in the absolute and

in the relative sense. However, we see that the extra water vapour "added" from HALOE above 30km produces a slight *increase* in longwave adjusted forcing, despite the significant cooling it causes in the upper stratosphere. This may seem peculiar, but is in fact just another indication of the small radiative importance (in terms of SWV) attributable to regions above 30km. The increased emission from regions above 30km clearly leads to a local cooling as well as to a slight increase in lower stratospheric warming. It is the latter that once again dominates in terms of radiative forcing, hence the net increase in LW adjusted forcing.

Chapter 4

Summary

The main focus in this thesis has been on the anthropogenic contributions to the increase in stratospheric water vapor: methane oxidation and emissions from air traffic. The observed increase in recent decades is also thought to express feedbacks from climate changes affecting the natural mechanisms responsible for bringing water vapor into the stratosphere. However, such eventual changes along with their consequences for the levels of SWV are poorly understood, and was considered a topic well beyond the scope of this work.

Our findings were summarized in three principal sections: one dealing with idealized water vapor perturbations, the second with air traffic emission scenarios and the last with various methods of estimating the impact of methane oxidation.

As for the model runs involving the idealized perturbations, these turned out to provide useful results in several aspects, despite their eventual lack in absolute realism in expressing observed changes in SWV. Firstly, the procedure of perturbing an everywhere fixed background SWV value of 6 ppmv by 0.7 ppmv is among the most widely used experimental setups referred to in published results. Thus, this provides a unique possibility of intercomparing calculated forcings with the findings of other researchers. This was done preliminarily by using single-profile versions of the disort and OBIR models, thereby at the same time validating the models' abilities to properly model atmospheric radiative transfer. Our net forcing of 0.156 W/m^2 calculated in full T21L60 resolution (listed in Table 4.1) is in fair agreement with the 0.19 W/m^2 net forcing calculated in **?**. Furthermore, we chose to use the uniform perturbation scheme as a basis for several sensitivity tests, involving both the perturbation of water vapor in single layers and the removal of tropospheric water vapor. The main purpose of these tests was to thoroughly investigate the stratospheric temperature response modeled by the everywhere uniform 0.7 ppm perturbation applied previously. The single layer perturbations clearly demonstrated the domination of the lowermost stratospheric regions in affecting the adjusted radiative forcing, as well as the theoretical potential for lower stratospheric warmings by perturbations in higher layers. However, the results from these sensitivity studies proved to be more than just educational examples by later representing highly useful tools during the analyses of temperature responses from methane oxidation.

Turning to the air traffic emission scenarios described in section 3.2, these were shown to have a rather limited impact in terms of radiative forcings from increased water vapor levels. The largest of the four derived instantaneous long-wave forcings was as low as 0.048 W/m^2. Although stratospheric temperature adjustment was not carried out, we can conclude, based on results from the sensitivity test runs, that the net forcings from these emissions are unlikely to greatly exceed their instantaneous value. In fact, the subsonic cases will most probably give net forcings below their instantaneous values, due to the emissions being situated directly above the local tropopause. Thus, in order to tie these future scenarios to aircraft emissions of SWV during the past 50 years, we may generally think of the value referred to as "Subsonic 2050" listed in Table 4.1 as a realistic upper bound , since this (instantaneous) forcing is based on changes in air traffic that, at least in terms of water vapor emissions, resemble those seen between the onset of large-scale commercial air traffic and present day conditions.

Finally, the focus was put on the second known anthropogenic source of SWV: the oxidation of stratospheric methane. Through the use of observational (HALOE) and modeled (CTM) data, used both separately and in combination, we established a number of forcing estimates for various periods of time, as listed in Table 4.1. Clearly, the use of CTM data did not contribute as much as initially hoped to the narrowing down of these final estimates. As was seen in Figure 3.12 d), the differences between the two types of datasets proved to be substantial in certain regions, most likely due to an under-representation of the effect of stratospheric chlorine by the CTM. The first runs carried out were the ones dealing with preindustrial to present-day changes, giving radiative forcings of between 0.061 W/m^2 and 0.077 W/m^2 for 1850-2000, and a HALOE-based estimate of 0.083 W/m^2 for 1750-2000. Comparing this with radiative forcings from "traditional" greenhouse gases, the latter estimate makes up 5.7% of the forcing from CO_2, 18% of the forcing from methane and 55% of the forcing from N_2O, using values from IPCC (2001)

Besides the calculation of radiative forcings, some interesting results were found when studying stratospheric temperature responses modeled from the imposed methane-induced changes. The generated water vapor change fields indicated a strong dependence of the magnitude of stratospheric coolings on the vertical profile of the increase in water vapor. Most notably, water vapor profiles associated with methane oxidation were shown to be capable of inducing warmings in the lower stratosphere. This indicates that there is not necessarily a contradiction between substantial SWV increases and moderate or even negative stratospheric coolings as long as certain criteria are fulfilled by the vertical profile of the water vapor change. Attempts to further generalize the link between vertical SWV profiles and stratospheric temperature responses was considered to lay outside the scope of this thesis, but could well be a topic of future work.

Bearing in mind the estimate presented in Forster and Shine (2002) of a radiative forcing of as much as 0.60 W/m^2 calculated from all reliable time-series of observed increases in SWV since 1960, methane oxidation seems to be a rather modest contributor to the overall increase in this period.

However, given that the estimate of Forster & Shine is correct, our forcing estimate of 0.050 W/m^2 for the period 1950-2000 makes up 8 % of the total forcing, which is far from insignificant. Adding the contribution from air traffic, we may end up somewhere in the vicinity of 10%. This confirms that the radiative forcing derived from observed increases in the concentrations of stratospheric water vapour is partly to be considered as a direct anthropogenic forcing on the climate. However, the main part of this much-debated increase remains unexplained, and given the possibly large associated radiative forcing, stratospheric water vapor should have a potential for attracting interest from the scientific community in years to come.

Simulation	**Net forcing**
6ppmv to 6.7 ppmv	0.156 W/m^2
"Sub+super 2050"	0.048[1] W/m^2
"Subsonic 2050"	0.017[1] W/m^2
HALOE 1750-2000	0.083 W/m^2
HALOE 1850-2000	0.077 W/m^2
HALOE 1950-2000	0.050 W/m^2
CTM+zero 1850-2000	0.061 W/m^2
CTM+HALOE 1850-2000	0.063 W/m^2

Table 4.1: Summary of results from selected model runs

[1] LW instantaneous forcing

Bibliography

Ewards, J.M. and Slingo, A. (1996) *Studies with a flexible new radiation code. I: Choosing a configuration for a large-scale model*. Q.J.R. Meteorol. Soc., volume 122:pp. 689–719.

Forster, P.M. de F.; Ponater, M. and Zhong, W. (2001) *Testing broadband radiation schemes for their ability to calculate the radiative forcing and temperature response to stratospheric water vapor and ozone changes*. Meteorol. Z., volume 10:pp. 387–393.

Forster, P.M. de F. and Shine, K.P. (1999) *Stratospheric water vapour changes as a possible contributor to observed stratospheric cooling*. Geophysical research letters, volume 26(21):pp. 3309–3312.

Forster, P.M. de F. and Shine, K.P. (2002) *Assessing the climate impact of trends in stratospheric water vapour*. Geophysical research letters, volume 29:p. 10.1029/2001GL013 909.

Gauss, M.; Isaksen, I.S.A.; Wong, S. and Wang, W.C. (2003) *Impact of H2O emissions from cryoplanes and kerosene aircraft on the atmosphere*. Journal of geophysical research, volume 108(D10):p. 4304.

Graf, H.F; Kirchner, I and Perlwitz, J. (1998) *Changing lower stratospheric circulation: The role of ozone and greenhouse gases*. J. Geophys. Res., volume 103(D10):pp. 11 251–11 262.

IPCC (1999b) *Aviation and the global Atmosphere. Summary for Policymakers*. Intergovernmental Panel on Climate Change, Cambridge University Press.

IPCC (2001) *Third Assessment Report - Climate Change 2001*. The third assessment report of the intergovernmental panel on climate change, IPCC/WMO/UNEP.

Liou, V.N (2002) *An introduction to Atmospheric Radiation*. International geophysics series, volume 84 (Academic Press).

Myhre, G. (1998) *Radiative forcing of climate: Effects of changes in well mixed greenhouse gases, ozone and aerosols*. Ph.D. thesis, University of Oslo.

Myhre, G.; Highwood, E.J.; Shine, K.P. and Stordal, F. (1998) *New estimates of radiative forcing due to well mixed greenhouse gases*. Geophysical research letters, volume 25(14):pp. 2715–2718.

Myhre, G. and Stordal, F. (1997) *Role of spatial and temporal variations in the computation of radiative forcing and GWP*. journal of geophysical research, volume 102(D10):pp. 11,181–11,200.

Oinas, V.; Lacis, A.A.; Rind, D.; Shindell, D.T. and Hansen, J.E. (2001) *Radiative cooling by stratospheric water vapour: big differences in GCM results*. Geophysical research letters, volume 28(14):pp. 2791–2794.

Petty, G.W. (2004) *A first course in atmospheric radiation* (Sundog publishing).

Rosenlof, K.H.; Oltmans, S.J.; Kley, D.; Russell III, J.M.; Chiou, E.W.; Chu, W.P.; Johnson, D.G.; Kelly, K.K.; Michelsen, H.A.; Nedoluha, G.E.; Remsberg, E.E.; Toon, G.C. and McCormick, M.P. (2001) *Stratospheric water vapour increases over the past half-century*. Geophysical research letters, volume 28(7):pp. 1195–1198.

SCENIC (2005) *Scenario of aircraft emissions and impact studies on chemistry and climate*. Final report, Project number EVK2-2001-00103.

Shine, K.P.; Bourqui, M.S.; Forster, P.M. de F.; Hare, S.H.E.; Langematz, U.; Braesicke, P.; Grewe, V.; Ponater, M.; Schnadt, C.; Smith, C.A.; Haigh, J.D.; Austin, J.; Butchart, N.; Shindell, D.T.; Randel, W.J.; Nagashima, T.; Portmann, R.W.; Solomon, S.; Seidel, D.T.; Lanzante, J.; Klein, S.; Ramaswamy, V. and Schwartzkopf, M.D. (2003) *A comparison of model-simulated trends in stratospheric temperatures*. Q.J.R.Meteorol. Soc., volume 129:pp. 1565–1588.

Smith, C.A.; Haigh, J.D. and Toumi, R. (2001) *Radiative Forcing due to Trends in Stratospheric Water Vapour*. Geophysical research letters, volume 28(1):pp. 179–182.

Stamnes, K.; Tsay, S.C.; Wiscombe, W. and Jayaweera, K. (1988) *Numerically stable algorithm for discrete-ordinate-method radiative transfer in multiple scattering and emitting layer media*. Applied optics, volume 27(12):pp. 2502–2509.

Stordal, F. (1988) *A wide band model for transfer of infrared radiation: altitudinal,latitudinal and yearly variation of cooling rates in the troposphere and the stratosphere.*. Technical Report 68, Institute for Geophysics, University of Oslo.

WMO (1998) *Scientific assessment of ozone depletion*.

Zhong, W. and Haigh, J.D. (2003) *Shortwave radiative forcing by stratospheric water vapour*. Geophysical research letters, volume 30(3):p. 1113.

Zhong, W.; Haigh, J.D.; Belmiloud, R.; Schermaul, R. and Tennyson, J. (2001a) *The impact of new water vapour spectral line parameters on the calculation of atmopsheric absorption*. Q.J.R. Meteorol. Soc., volume 127:pp. 1615–1626.